Kaunas University of Technology

Faculty of Mathematics and Natural Sciences

Development of Recommendations for the Quality Control of Magnetic Resonance Imaging in Lithuanian Health Care Institutions

Master's Final Degree Project

Gustė Laurikaitytė

Project author

Prof. Dr. Diana Adlienė

Supervisor

Kaunas, 2025

Kaunas University of Technology

Faculty of Mathematics and Natural Sciences

Development of Recommendations for the Quality Control of Magnetic Resonance Imaging in Lithuanian Health Care Institutions

Master's Final Degree Project

Medical physics (6213GX001)

Gustė Laurikaitytė

Project author

Prof. Dr. Diana Adlienė

Supervisor

Prof. Dr. Liutauras Marcinauskas

Reviewer

Kaunas, 2025

Kaunas University of Technology

Faculty of Mathematics and Natural Sciences

Gustė Laurikaitytė

Development of Recommendations for the Quality Control of Magnetic Resonance Imaging in Lithuanian Health Care Institutions

Declaration of Academic Integrity

I confirm the following:

1. I have prepared the final degree project independently and honestly without any violations of the copyrights or other rights of others, following the provisions of the Law on Copyrights and Related Rights of the Republic of Lithuania, the Regulations on the Management and Transfer of Intellectual Property of Kaunas University of Technology (hereinafter – University) and the ethical requirements stipulated by the Code of Academic Ethics of the University;

2. All the data and research results provided in the final degree project are correct and obtained legally; none of the parts of this project are plagiarised from any printed or electronic sources; all the quotations and references provided in the text of the final degree project are indicated in the list of references;

3. I have not paid anyone any monetary funds for the final degree project or the parts thereof unless required by the law;

4. I understand that in the case of any discovery of the fact of dishonesty or violation of any rights of others, the academic penalties will be imposed on me under the procedure applied at the University; I will be expelled from the University and my final degree project can be submitted to the Office of the Ombudsperson for Academic Ethics and Procedures in the examination of a possible violation of academic ethics.

Gustė Laurikaitytė

Confirmed electronically

Laurikaitytė Gustė. Development of Recommendations for the Quality Control of Magnetic Resonance Imaging in Lithuanian Health Care Institutions. Master's Final Degree Project / supervisor Prof. Dr. Diana Adlienė; Faculty of Mathematics and Natural Sciences, Kaunas University of Technology.

Study field and area (study field group): Medical Technologies (Health Sciences).

Keywords: Magnetic Resonance Imaging, quality control.

Kaunas, 2025. 63 pages

Summary

Magnetic resonance imaging (MRI) along with computed tomography (CT) is a gold standard for diagnosis of lesions. It is known that diagnostic procedures are strictly regulated, and quality control (QC) is a part of these regulations. However, Lithuania lacks official national QC regulations for MRI and every clinic is trying to overcome this regulatory gap using its own MRI scanning protocol, most often following existing American standards providing functional standardized quality assurance protocols to fill this regulatory void.

This investigation is aimed at creating and validating an MRI quality control (QC) protocol which can be used in Lithuanian clinical environments. The investigation relies on the phantom based QC measurements performed evaluating three MRI scanners: Siemens Magnetom Skyra (3T), Siemens Magnetom Altea (1.5T), and Philips Ingenia Prodiva (1.5T). Following phantom based QC tests have been performed: measurements of signal-to-noise ratio (SNR), image uniformity (PIU), geometric distortion, low-contrast detectability and high-contrast spatial resolution. The obtained results matched with American OC standards showing just minor variations among devices and sequences. This allowed for development of the unified recommendations for the creation of national MRI QC protocol. The implementation of such protocol would lead to the uniform requirements for image quality, diagnostic dependability and better patient protection throughout the country.

Laurikaitytė Gustė. Branduolių magnetinio rezonanso vaizdinimo kokybės patikros rekomendacijų parengimas Lietuvos gydymo įstaigoms. Magistro baigiamasis projektas / vadovė prof. dr. Diana Adlienė; Kauno technologijos universitetas, Matematikos ir gamtos mokslų fakultetas.

Studijų kryptis ir sritis (studijų krypčių grupė): Sveikatos mokslai, Medicinos technologijos.

Reikšminiai žodžiai: MRT, kokybės kontrolė.

Kaunas, 2025. 63 p.

Santrauka

Magnetinio rezonanso tomografija (MRT), kaip ir kompiuterinė tomografija (KT), yra laikoma vienu pagrindinių šiuolaikinės diagnostikos standartų. Žinoma, kad diagnostinės procedūros yra griežtai reglamentuojamos, o kokybės kontrolė sudaro esminę šių reglamentų dalį, užtikrinančią tyrimų tikslumą ir pacientų saugumą. Vis dėlto Lietuvoje šiuo metu nėra patvirtintų oficialių nacionalinių MRT kokybės kontrolės reikalavimų. Dėl šios priežasties kiekviena gydymo įstaiga savarankiškai sprendžia šį trūkumą, taikydama individualius MRT skenavimo protokolus. Dažniausiai vadovaujamasi jau egzistuojančiais Amerikos standartais, kurie siūlo funkcinius ir standartizuotus kokybės užtikrinimo sprendimus.

Šio tyrimo tikslas – sukurti ir patvirtinti MRT kokybės kontrolės protokolą, kuris galėtų būti taikomas Lietuvos klinikinėje praktikoje. Šis tyrimas remiasi fantomų grįstais kokybės kontrolės matavimais, atliktais naudojant tris skirtingus MRT aparatus: Siemens Magnetom Skyra (3T), Siemens Magnetom Altea (1,5T) ir Philips Ingenia Prodiva (1,5T). Vertinimui buvo taikomi šie kokybės kontrolės testai: signalo ir triukšmo santykio (angl. *signal-to-noise ratio*, SNR), vaizdo vienodumo (angl. *image uniformity*, PIU), geometrinio iškraipymo, mažo kontrasto aptikimo bei didelio kontrasto erdvinės raiškos matavimai. Gauti rezultatai buvo palyginti su Amerikos kokybės kontrolės standartais – nustatyti tik nežymūs skirtumai tarp įrenginių ir skenavimo sekų. Šie rezultatai sudarė pagrindą rengti rekomendacijas dėl nacionalinio MRT kokybės kontrolės protokolo kūrimo Lietuvoje. Tokio protokolo įdiegimas leistų suvienodinti vaizdo kokybės, diagnostinio patikimumo bei pacientų saugos reikalavimus visos šalies mastu.

Table of contents

List of figures

List of tables

List of abbreviations

Abbreviations:

MRI – magnetic resonance imaging;

QC – quality control;

SNR – signal-to-noise ratio;

PIU – percent image uniformity;

ACR – American College of Radiology;

AAPM – American Association of Physicists in Medicine;

IEC – International Electrotechnical Commission;

NEMA – National Electrical Manufacturers Association;

FDA – Food and Drug Administration;

CT – computed tomography;

NMR – Nuclear Magnetic Resonance

GRE – Gradient Echo;

RF – radiofrequency

TE – echo time;

TR – repetition time;

DWI – diffusion-weighted imaging;

MRA – magnetic resonance angiography;

SAR – specific absorption rate;

PLA – printed polylactic acid.

Introduction

The diagnostic field of modern medicine relies heavily on Magnetic Resonance Imaging (MRI) because it creates comprehensive three-dimensional images of soft tissues using non-ionizing radiation technologies [1]. Due to the complexity and sensitivity of new technologies, MRI quality and consistency is very important step. Quality control (QC) in MRI involves periodic performance assessments through standardized test phantoms together with image quality metrics including signal-to-noise ratio (SNR), percent image uniformity (PIU), ghosting and geometric accuracy. The quality measures serve to detect system deterioration while enabling hardware component calibration and image quality optimization throughout time. The American College of Radiology (ACR) together with the American Association of Physicists in Medicine (AAPM) and the International Electrotechnical Commission (IEC) have established worldwide standards for QC practices through their guidelines [2, 3]. In Lithuania, where this study is based, currently there is no official national standards for MRI quality control except for annual service engineer inspections. The absence of structured QC programs in many facilities usually lead to suboptimal imaging and undetected system malfunctions and inconsistent diagnostic performance [4].

This project is aimed at creating recommendations for establishing of unified national MRI quality control (QC) protocol which can be used in Lithuanian health care institutions.

The tasks:

1. To perform and analyse a phantom-based MRI quality control (QC) measurements for different MRI machines, comparing the data obtained using various scanning protocols.
2. To compare and analyse obtained results based on European and American regulatory standards.
3. To develop recommendations for establishing national MRI QC protocol for clinical applications.

1. Literature review

1.1. Magnetic resonance imaging

Magnetic resonance imaging (MRI) is a non-invasive medical imaging technique that produces high-resolution, three-dimensional images of the internal body structures. It uses strong magnetic fields and radio waves to excite and detect proton spinning changes in living tissues [1]. Also, MRI is commonly used to diagnose diseases, evaluate tissue abnormalities, and monitor treatment progress. It provides detailed insights into soft tissues and non-bony structures, allowing for better viewing of the brain, spinal cord, nerves, muscles, ligaments, and tendons. It can detect joint damage, inflammation, soft tissue injuries, internal organ diseases, tumours, signs of stroke, dementia, neoplasm and etc. It also offers in-depth analysis into metabolism, function, and molecular structure, expanding applicability of MRI method in a variety of fields. It has accelerated progress in quantitative imaging for precision medicine, functional MRI for brain activity analysis and fibre tracking in neuroradiology [5]. Comparing the difference with other imaging modalities, MRI differs from X-rays and computed tomography (CT) by producing detailed images of soft tissues and organs without the use of ionizing radiation. Because of this, MRI is preferred imaging modality for frequent diagnostic or therapeutic imaging, but it is more expensive compared to X-ray or CT imaging [1].

Another technology - ultrasound imaging - also does not use the ionizing radiation, but high-frequency sound waves that provide real-time insights of internal structures [6]. Ultrasound is used for real-time imaging, emergency assessments, and pregnancy monitoring because of its speed, mobility, and safety.

MRI is the golden standard for identifying complicated lesions including brain tumours and spinal injuries (Fig. 1) [6].

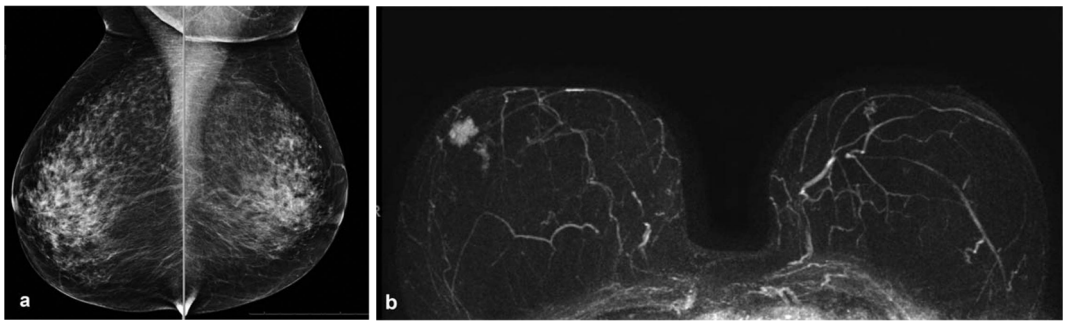

Fig. 1. Difference between digital mammography (a) and breast MRI (b) from the same patient. The mammogram shows heterogeneously dense breasts, while breast MRI reveals an invasive breast cancer, along with a ductal carcinoma in situ (DCIS) [7]

Adverse effects related to MRI scans are extremely rare. Each year, over 40 million MRI scans are performed in the United States [8], with the Food and Drug Administration (FDA) receiving roughly 300 adverse event reports involving MRI scanners and coils. These reports arise from manufacturers, distributors, hospitals, and patients. The most common complaints reported to the FDA are heat injury, including second-degree burns [5]. Other recorded accidents include projectile-related injuries (items being dragged toward the MRI scanner), crushed or pinched fingers from the patient table, falls, and auditory problems including hearing loss or tinnitus [5]. Furthermore, the FDA has raised concerns regarding the poor appearance and quality of MRI images.

Given potential risks, quality control (QC) is crucial to assuring safety and effectiveness as well as maintaining the accuracy and reproducibility of MRI equipment. By monitoring scanner performance and using phantoms for calibration, QC ensures that MRI systems produce precise and reliable data [9]. QC plays a crucial role in detecting potential safety issues such as excessive radiofrequency heating, gradient malfunctions, also periodic monitoring reduces the possibility of technical problems that could result in picture degradation or patient harm. Additionally, standardized protocols and repeatability testing help maintain consistency across different locations over time, which is essential for multicentred research and longitudinal analysis [10].

1.2. Basic Principles of Magnetic Resonance Imaging Physics

Nuclear Magnetic Resonance (NMR) is the physical phenomenon in which atomic nuclei in a magnetic field absorb and re-emit electromagnetic radiation. Its ability to provide detailed molecular insights allows for discoveries in medical imaging (MRI), biochemical analysis, structural determination, quality control, and material characterization, making it essential in both scientific and industrial sectors [11]. NMR is based on the interaction of nuclear spins with an external magnetic field, resulting in energy absorption and emission. The quantum mechanical property of spin angular momentum (Fig. 2 (A)), in protons and other atomic and subatomic particles causes them to behave like small magnets [12]. The spin angular momentum of a rotating object has both a specific direction and a fixed magnitude. This magnitude is quantized, which means it can only exist in discrete quantities like whole numbers or half-integers [12]. The spins" cancel out" in nuclei with an even number of protons and neutrons, resulting in zero net spin, which cannot be seen by MRI [12]. Standard MRI relies on the hydrogen nucleus, which has a single proton in its nucleus with a spin value of ½ found in all tissues in the body, including water, fat, muscles and chemical molecules. Hydrogen, is both sensitive to NMR and abundant in tissues, making it necessary for MRI signal generation [13]. In the absence of an external magnetic field, proton spins are in random orientations due to thermal energy, yielding no net magnetization in either direction (Fig. 2 (B)). Spins interact and align with a strong static magnetic field (B_0) in an MRI scanner, resulting in a small net magnetization (M_0) along the field direction [12] (Fig. 2 (C)). This alignment arises because nuclear spins can occupy one of two energy states: aligned with the B_0 (low-energy state) or opposed to it (high-energy state), with a minor excess of protons in the lower-energy state, leading to a net magnetization [14].

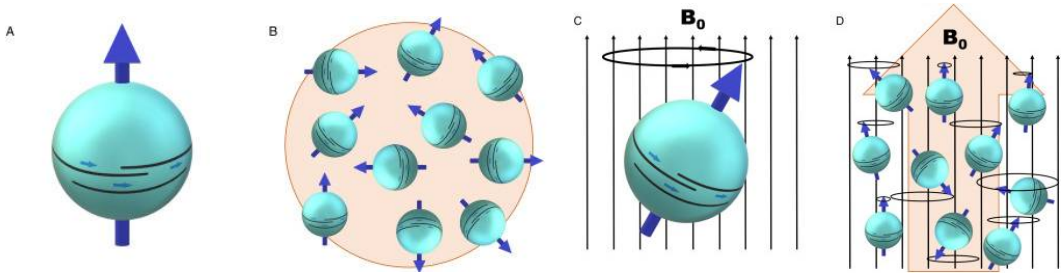

Fig. 2. (A) A proton "spins" around its magnetic dipole's axis; (B) When not subjected to a strong magnetic field, the proton spins randomly in either direction, causing no net magnetization (orange sphere); (C) Proton alignment with B_0 and precession around B_0 static magnetic field direction; (D) Spins align with B_0 to create a net magnetization (orange arrow) in the direction of B_0 [15]

Protons do not just align with B_0 but also precess around its axis due to the torque generated by their intrinsic magnetic moment interacting with the external field. This precession can be explained using

the gyroscope analogy, in which a spinning top does not remain exactly upright but instead tips off-centre and travels in a circular motion when viewed from above [12]. Similarly, proton spins precess around B_0 rather than their own rotational axis, indicating that they revolve at different angles relative to it. So, instead of remaining stable, the nuclei precess around the B_0 axis at a frequency known as the Larmor frequency, which is exactly proportional to the strength of the external field and represented by the Larmor equation (Eq. 1) [14]:

$$\omega_0 = \gamma \cdot B_0 \tag{1}$$

where: ω_0 – Larmor frequency [in rad/s]; γ – gyromagnetic ratio [in MHz/T]; B_0 – the applied magnetic field strength [in T].

The Larmor frequency is the rate at which a charged particle's magnetic moment, such as a proton, precesses around an external magnetic field [14]. In MRI, this frequency is critical because it defines the resonance frequency of hydrogen nuclei in the body, allowing for precise signal creation and image development [14]. Increasing B_0 causes an increase in Larmor frequency, affecting signal detection and resolution. In clinical MRI scanners, various field strengths of 1.5T, 3T, and 7T are used to optimize image quality and contrast.

In MRI, resonance occurs when an external radiofrequency pulse matches the Larmor frequency of hydrogen nuclei, causing them to absorb energy and modify their alignment to a higher energy state. When an RF pulse of the Larmor frequency is applied, protons absorb the energy. This causes their net magnetization vector to shift away from alignment with B_0, shifting from a low-energy state (parallel to B_0) to a high-energy one (anti-parallel) (Fig. 3) [16]. During scanning, an oscillating RF pulse, B_1, is delivered perpendicular to B_0 and rotates with the same frequency as proton precession. This allows energy transmission from the RF pulse to the protons. Consequently, the net magnetization (M) shifts from the longitudinal (z) axis to the transverse (xy) plane and continues to precess around B_0 [12]. On the macroscopic level, this action causes the longitudinal net magnetization (M_0) to be temporarily lost, while a new transverse net magnetization (M_{xy}) is formed, sweeping back and forth in the transverse plane [16]. The flip angle of rotation is controlled by the strength and duration of the RF pulse. The RF pulse alters the spins' orientation relation to B_0, but not their orientation relative to each other. Instead, it rotates the entire set of spins together [12]. This means that the few spins that were originally aligned parallel with B_0 keep their alignment but collectively rotate to become non-parallel with B_0. These protons now precess in phase in the transverse (xy) plane, which results in a net magnetization (M_{xy}) (Fig. 3) [12]. This resonance phenomenon is essential in MRI because it enables protons to be excited and release measurable signals, which are then used to create detailed images of tissues.

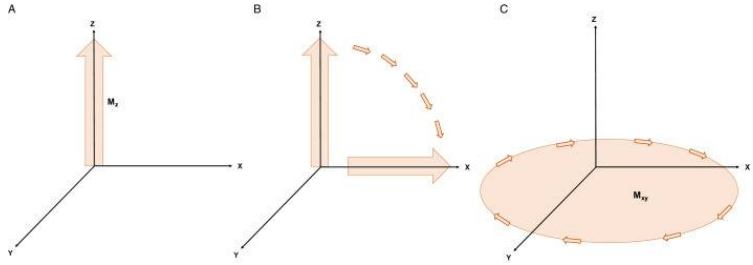

Fig. 3. (A) The net magnetisation M_z aligns with B_0 without precession; (B) RF pulse tips the net magnetisation M into traverse plane (90° shown); (C) The net magnetisation M_{xy} precesses, generating a signal in the receiver coil [15]

1.2.1. Spin relaxation and echoes

Once the RF pulse is turned off, the excited spins do not stay in a high-energy state indefinitely. Instead, they begin to return to their original equilibrium state through relaxation processes, which are essential for MRI signal detection and picture contrast. In MRI, this relaxation happens through two mechanisms: T_1 (longitudinal) and T_2 (transverse). These mechanisms control how signals are detected and affect picture contrast:

- ***T_1* Relaxation** (Spin-Lattice Relaxation) protons return to equilibrium by transferring absorbed energy to their surrounding molecular environment (the lattice), resulting in the recovery of longitudinal magnetization. T_1 relaxation differs between tissues, impacting MRI contrast: fat (shorter T_1) looks bright, whereas fluids (longer T_1) seem dark. T_1-weighted imaging detects cancers, haemorrhages, and contrast-enhanced lesions [17].

- ***T_2* Relaxation** (Spin-Spin Relaxation) refers to the progressive loss of transverse magnetization caused by dephasing interactions between nearby proton spins, without energy loss to the surrounding environment. Longer T_2 tissues (e.g., fluids) retain signal and look bright, whereas shorter T_2 tissues (e.g., fat,./ muscle) quickly lose signal and appear dark. *T_2-weighted* imaging is crucial for identifying edema, inflammation, and lesions linked with high water content [17].

Although energy recovery and spin-spin interactions are described by T_1 and T_2 relaxation, respectively, the impact of external magnetic field inhomogeneities is not taken into consideration. T_2* (T_2 star) (Fig. 4). Relaxation time describes rapid decay of transverse magnetization caused by magnetic field inhomogeneities and spin-spin interactions. These inhomogeneities might arise from tissue properties (e.g., iron accumulation, microhaemorrhages) or problems with the MRI machine's magnetic field [18]. T_2* relaxation causes faster signal loss than T_2 relaxation due to magnetic field inhomogeneities. These inhomogeneities cause protons to precess at slightly different frequencies, resulting in phase decoherence and a faster transverse magnetization decay. T_2* weighted imaging, especially in Gradient Echo (GRE) sequences, detects iron deposits in the liver, haemorrhages, and tissue susceptibility changes [18]. Standard T_2 imaging (using Spin Echo sequences) lowers inhomogeneity effects, resulting in better soft tissue contrast. T_2* relaxation causes rapid signal loss due to dephasing from magnetic field inhomogeneities, hence MRI employs many strategies to correct or use this issue.

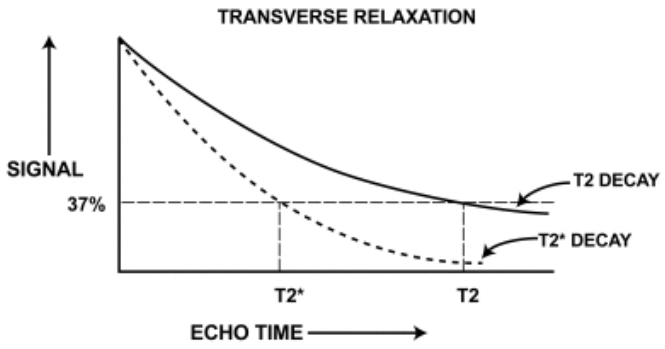

Fig. 4. Comparison of $T_2$and T_2*Transverse Relaxation Curves in MRI [19]

To help recover or use the decaying signal, generating effective contrast in MRI images, echo formation methods, such as Spin Echo (SE) and Gradient Echo (GRE) are used. These echo formation methods have a distinct function in the processing of MRI signals:

- **Free Induction Decay (FID)** is the initial signal produced immediately after an RF pulse excites the hydrogen nuclei, generating transverse magnetization. The FID signal is a sine wave that decays exponentially over time, regulated by the T_2* constant [15]. This decay is caused by proton spin dephasing because of magnetic field inhomogeneities. While FID serves as the foundation for signal capture in MRI, it is rarely used for image formation due to its high signal loss.

- **Spin Echo (SE)** is formed by applying a 90° excitation pulse, which shifts net magnetization into the transverse plane, followed by a refocusing pulse of 180° that reverses dephasing produced by T_2* effects (Fig. 5 (left)) [20]. This refocusing creates an "echo" of the original signal. Echo time (TE) is the interval between the peak of the initial RF pulse and the midpoint (peak) of the resulting echo signal and repetition time (TR) is the time between two consecutive RF excitation pulses [15]. SE sequences improve *T_2-weighted* imaging by adjusting for field inhomogeneities, resulting in better tissue contrast.

- **Gradient Echo (GRE)** is generated by reversing the polarity of magnetic field gradients to refocus dephased spins without the need of a 180° RF pulse (Fig. 5 (right)). Following excitation with an RF pulse, a dephasing gradient is applied, followed by an opposite-polarity rephasing gradient, creating an echo [21]. Unlike SE, GRE does not reduce T_2* effects, making it more vulnerable to magnetic field inhomogeneities and susceptibility artifacts. Because of shorter TR, the acquisition time is faster, so, GRE is commonly used in functional MRI (fMRI), cardiac imaging, and angiography [21].

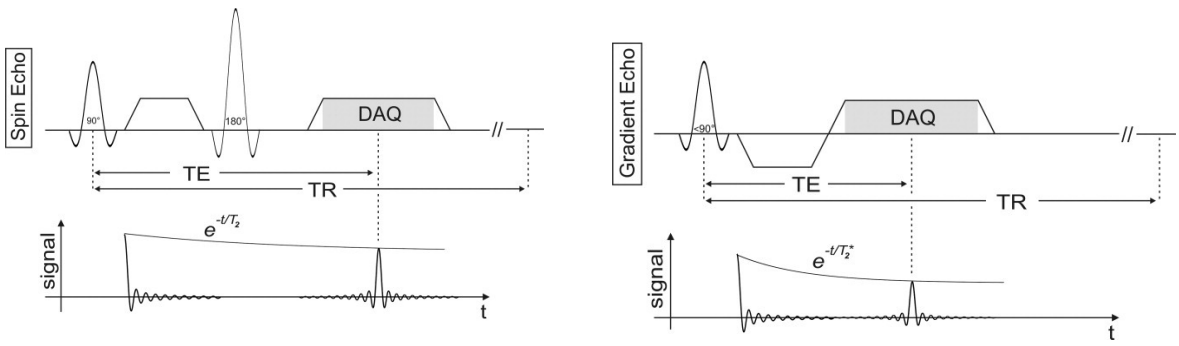

Fig. 5. Spin echo (left) employs a 180° refocusing pulse, whereas gradient echo (right) creates an echo using only one RF pulse and gradient reversal. T_2 star effects cause gradient echo signals to decay quicker, whereas spin echo maintains T_2 contrast by correcting for field inhomogeneities. DAQ stands for data acquisition time [21]

Echo creation methods like Spin Echo and Gradient Echo are vital for recovering and exploiting MRI signals (managed by T_2 and T_2* effects), other approaches like Inversion Recovery (IR) refine tissue contrast by selectively suppressing certain signals based on T_1 relaxation features. Inversion recovery is an advanced MRI method that enhances tissue contrast by using variations in T_1 relaxation times [22]. It accomplishes this by introducing a 180° inversion pulse before the typical spin echo pattern. Tissues recover magnetization at various rates during inversion times (TI), allowing for selective suppression or amplification. Two main types are Short Tau Inversion Recovery (STIR), which suppresses fat and is effective for edema, inflammation, and tumours, and Fluid-Attenuated Inversion

Recovery (FLAIR), which suppresses cerebrospinal fluid and improves brain lesion detection [23]. IR is utilized for musculoskeletal, whole-body, and neurological imaging.

1.2.2. Image generation

Magnetic Resonance Imaging relies heavily on signal acquisition and k-space filling since they have a direct impact on acquisition time, resolution, and image quality. The MR signal is generated when body's excited hydrogen nuclei relax and emit electromagnetic waves, which receiver coils detect. This signal is a continuous wave with frequency and phase gradients encoding spatial information [24]. To create discrete data points, the continuous MR signal is sampled and digitalized, with each point representing magnitude and phase values, or complex numbers with real and imaginary components.

All magnetic resonance image data first is obtained in the spatial frequency domain, known as k-space. The k-space is a two-dimensional (2D) matrix containing information on signal frequencies and phases, which is an abstract concept rather than a physical place in the MRI machine [25]. K-space is a matrix where near the centre are low spatial frequencies, such as contrast and gross anatomy, while the periphery contains high spatial frequencies, such as edges and tiny details [26]. The MRI operator can modify the acquisition and manipulation of k-space data to affect the reconstructed image by varying parameters such acquisition speed, contrast, field of view, spatial and temporal resolution, and artifact reduction [24]. Information is stored line by line in k-space whenever an echo is acquired through phase and frequency encoding. This raw k-space data is obtained straight from the scanner before any processing or application of the Fourier transform. So, in the k-space, a point does not match a point in the image; rather, the central lines establish contrast, while the periphery lines carry information about spatial resolution [25]. By converting the k-space data into a spatial domain representation, a 2D Fourier transform gives the final reconstructed image.

In order to localize signals in three dimensions, MRI spatial encoding requires three crucial steps - slice selection, frequency encoding, and phase encoding:

- Slice selection – specifies which plane (axial, sagittal, or coronal) to scan. A slice selection gradient is used to choose a particular imaging slice during RF excitation. By altering the magnetic field along a single axis only protons in a specific slice resonate at the RF pulse frequency [27]. The slice thickness impacts both the gradient strength and the RF pulse bandwidth.

- Frequency encoding – is applied after slice selection, along the chosen axis during signal acquisition. Because of this frequency encoding gradient, protons at various locations precess at various frequencies, giving each body part a distinct frequency. These distinct frequencies are detected by the receiver coil, which helps with spatial localization by enabling signal differentiation along the frequency-encoded axis [28].

- Phase encoding – used to discriminate signals in a certain dimension between two RF pulses along the phase-encoding axis. Small phase shifts are produced in proton spins by applying a gradient field, which varies at various points along the selected axis. The spatial information is encoded by repeating this procedure over many TRs with varying gradient strengths. To help build an image, each phase encoding step covers a single line in k-space. The resolution increases with the number of phase encoding steps utilized, but the scan duration increases as well [15].

Given the circumstances, protons precess at various frequencies and phases at each spatial location due to the combination of gradient fields, frequency encoding and phase encoding gradients. This makes it possible to encode space precisely in every dimension. After that, the signal is saved in k-space for future image reconstruction.

In MRI echo time (TE) and repetition time (TR) are two crucial parameters that affect image contrast by controlling the strength of T_1 and T_2 relaxation effects. These factors establish whether the picture is T_1-weighted, *T_2-weighted* or proton density-weighted [29]. By influencing longitudinal relaxation, TR regulates *T_1-weighted* contrast meaning a shorter TR increases T_1 contrast. By affecting transverse relaxation, TE regulates *T_2-weighted* contrast - a longer TE increases T_2 contrast. A long TR and TE improve *T_2-weighted* contrast (Fig. 6), which is helpful for identifying diseases like inflammation and edema, while a short TR and TE create a *T_1-weighted* picture, which is perfect for seeing anatomical features.

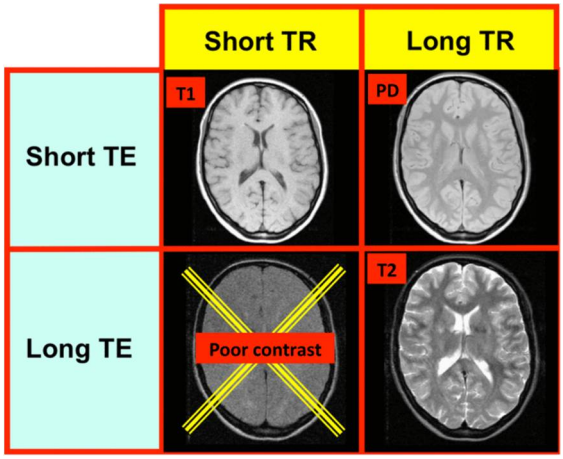

Fig. 6. Effect of TR and TE on MRI contrast [30]

In MRI image generation, anomalies such as distortions, signal voids, addition or removal of information are referred as artifacts [31] (Fig. 7). Artifacts in MRI are caused by motion, field inhomogeneities, aliasing, and susceptibility variations. Typical correction methods include fat suppression for chemical shift artifacts, anti-aliasing techniques (increased FOV), motion reduction techniques (gating, quicker sequences), and shorter TE or spin-echo sequences for susceptibility artifacts [31]. Adjusting parameters correctly reduces distortions and enhances image quality.

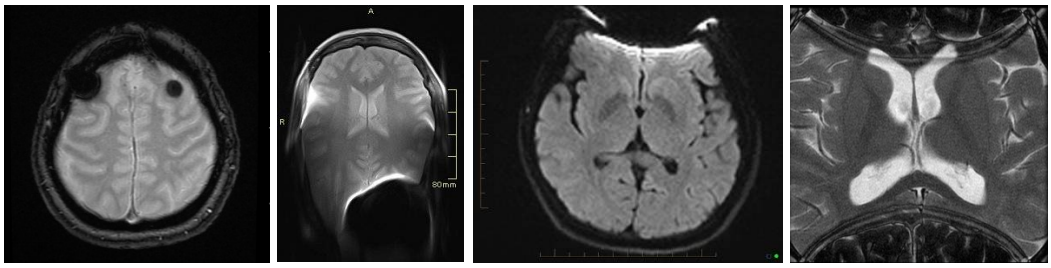

Fig. 7. Common MRI Artifacts [32]

Reducing artifacts improves image clarity, but signal-to-noise ratio (SNR) and resolution also affect image quality and need to be properly managed for the best imaging results. SNR is a critical determinant of MRI image quality, as it reflects the balance between the useful signal and background noise. While SNR affects diagnostic precision and the clarity of anatomical features, spatial resolution

determines the capacity for identifying small structures. While higher SNR increases clarity, it often requires longer scan durations or stronger fields. Voxel size affects resolution; smaller voxels increase detail but decrease SNR. For the best imaging, SNR and resolution must be balanced.

1.2.3. MR systems and their components

An MRI system consists of four basic components: the primary magnet, gradient coils, RF coils, and computer systems that run and connect the components (Fig. 8) [33].

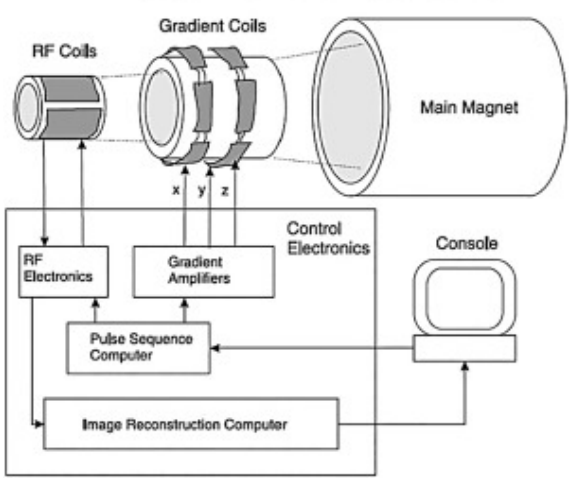

Fig. 8. MRI system components [34]

MRI system components:

- Magnets – the core of the MRI system, generating the static magnetic field. The production of high-quality images requires a magnetic field that maintains homogeneous across large volumes and consistent throughout time. Modern MRI system uses superconducting niobium-titanium magnets which operate at -263 °C in liquid helium to maintain continuous current flow for field generation [33]. The majority of clinical MRI systems operate at either 1.5T or 3T magnetic field strength with 3T being the most widely used because it offers optimal sensitivity and cost-effectiveness although 7T systems are used primarily for research applications [35].

- Gradients – provides for volume selection, spatial localization, and imaging in all planes by altering magnetic field strengths along the X, Y, and Z axes [36]. Gradient coil designs, such as saddle, birdcage, and linear, improve field efficiency and image quality while reducing artifacts. Shim coils are employed with gradients to address inhomogeneities un the B_0 field. The slew rate (mT/m/s) determines the speed at which gradients change, enabling faster sequences and better temporal resolution [37].

- Radiofrequency coils – broadcast radiofrequency pulses that excite protons and receive signals produced as protons return to equilibrium. These signals are translated into electrical impulses and used to create images [34]. Surface coils provide high SNR in shallow areas; volume coils provide more coverage; and phased-array coils improve SNR and resolution. Coil selection is based on clinical demands, anatomy, and field strength (1.5 T or 3 T), as mismatched coils might affect image quality [34]. Coil design influences signal-to-noise ratio, spatial resolution, and overall image quality.

- Computer system – coordinates subsystems, converts RF coil signals into digital data, and uses complex algorithms to reconstruct high-resolution images. Modern systems allow for real-time reconstruction, post-processing, and scan modifications, as well as integration with user terminals and hospital systems. Advanced technologies, such as parallel imaging, AI-based reconstruction, and noise reduction, increase efficiency and image quality [33].

1.2.4. Acquisition protocols

In MRI, different sequences provide unique types of contrast to highlight various tissues, structures and abnormalities. Standard MRI sequences:

- *T_1-weighted* Imaging – amplifies the signal of fatty tissue while suppressing the signal of water [38]. So, fat appears bright, and water appears dark. It is applied for detecting anatomical details and fat-containing structures.

- *T_2*-w*eighted* Imaging – improves the signal from the water, making it best for detecting fluid or edema [38].

- FLAIR (Fluid-Attenuated Inversion Recovery) – provides strong T_2 weighting, suppresses the CSF signal, and reduces the contrast between grey and white matter [39]. Improves visualization of brain abnormalities near fluid-filled areas.

- DWI (Diffusion-Weighted Imaging) – is a method for assessing the molecular function and microarchitecture of the human body [40]. Measures the diffusion of water molecules within tissue; sensitive to cellular changes. Areas with restricted diffusion appears white (certain tumours, acute stroke, etc.), areas with normal diffusion appears dark.

- MRA (Magnetic Resonance Angiography) – focuses on the body's blood vessels without the need for contrast (in most cases) [41]. Commonly used for evaluating blood flow in the arteries of brain, neck and kidneys.

But advanced MRI sequences allow for a much better depiction of the anatomy, tissue characterization, functional imaging and quantitative analysis. Advanced MRI sequences:

- Functional Magnetic Resonance Imaging (fMRI) – demonstrates regional, time-varying changes in brain metabolism [42]. With modified parameters can be used for spinal cord motor function [43].

- Spectroscopy – reveals the concentration of normal metabolites in a specific anatomic site and variations in those metabolites in the event of pathology [43]. Useful in identifying brain tumours, metabolic disorders, epilepsy and etc.

- Diffusion Tensor Imaging (DTI) – allows for the visualization of neuronal circuits and connectivity by capturing the direction and magnitude of water diffusion, making it a vital tool for understanding brain anatomy, function, and pathology [44].

1.3. Quality control in MRI

1.3.1. General issues

MRI requires quality control measures to ensure consistent results and precise outcomes which are essential for both research accuracy and diagnostic performance [45]. The use of substandard data leads to increased false positive and false negative rates in final results [46] which results in diagnostic errors, poor clinical decision-making (resulting in inappropriate therapies), research, clinical trial complications, reduced machine performance, lifespan, accreditation and compliance issues. The prevention of these problems requires the implementation of routine QA/QC procedures together with automated QC systems, regular maintenance, calibration, established imaging protocols, complete staff training, real-time system performance monitoring, adherence to regulatory criteria to ensure consistent image quality and correct diagnoses and optimal patient safety [47]. The maintenance of image quality through MRI quality control approaches consists of three categories: preventive, routine and corrective measures which function as essential components:

- **Preventive** QC system uses regular servicing and component checks with calibrations to prevent system problems from occurring before they start [48].
- **Routine** QC system performs continuous system performance checks through scheduled daily, weekly or monthly tests to sustain system performance [47].
- **Corrective** QC system repair detected faults to achieve optimal performance by addressing problems with artifacts, field inhomogeneity and coil failures.

The combination of standard QA procedures with preventive maintenance and daily/weekly coil inspections provides adequate quality control for standard clinical operations [47].

To complement these quality assurance techniques, several critical MRI quality control parameters are regularly evaluated:

- **Signal-to-Noise Ratio (SNR)** is a fundamental parameter which measures the clarity of MRI signal relative to background noise. Acceptance criteria for SNR are system specific due to variables as RF coil, scan conditions, and phantom, however values obtained during acceptance testing should be used as baseline references for continuous QA [49, 50]. SNR is calculated by dividing the mean signal intensity in a region of interest (ROI) inside the phantom by the standard deviation of the signal in a background ROI placed in the air outside the phantom (Eq. 2) [50]:

$$SNR = \frac{\bar{S}}{\sigma_{bkg}} \tag{2}$$

  where $\bar{S}$ is the signal, measured as the average of ROI intensities; σ_{bkg} is standard deviation of a background ROI.

- **Image Intensity Uniformity (PIU)** measures the consistency of signal intensity across the uniform region of phantom [50]. Poor signal homogeneity shows that the coil's image intensity varies substantially more than expected for a functioning system [51]. Inconsistent image intensity indicates a fault with the scanner, such as a defective volume coil or RF subsystems. Uniformity is measured in the brightest and darkest regions within phantom area. Uniformity is

defined as the difference between the maximum and minimum pixels in the ROI and results are displayed as a percentage of uniformity (PIU) (Eq. 3) [50]:

$$PIU = 100 \cdot \left(1 - \frac{S_{max} - S_{min}}{S_{max} + S_{min}}\right) \quad (3)$$

where S_{max} and S_{min} are the maximum and minimum pixel intensities in the area.

- **Contrast-to-Noise Ratio (CNR)** is a difference in signal intensity between two tissues (contrast) divided by the standard deviation for background noise. The higher the CNR the more likely the low-contrast lesion will be detected [52]. Lots of medical MRI research has been devoted to exploring ways to maximize this ratio in a wide range of disorders and situations (Eq. 4) [53]:

$$CNR = \frac{S_A - S_B}{S_{0w} N} \quad (4)$$

where S_A *and* S_B are the signal intensities from two different regions or tissue components in the image; S_{0w} is the fully recovered signal from water; N is noise voltage.

- **Spatial Resolution and Geometric Distortion** assesses the ability of a scanner to detect small objects and preserve correct spatial relationships. Failure of this test shows that the scanner cannot resolve fine details at the expected level for the given field of view and matrix size [51].

- **Ghosting and artifact assessment** allows for detection of undesirable image duplications or artifacts (such as ghosting and zipper artifacts) caused by hardware malfunction, RF interference, or motion. This topic will be discussed in the following section.

- **Gradient linearity and Eddy currents**. Gradient linearity corresponds to the exact variation of the gradient field with a distance; poor linearity results in a visual distortion, especially at the edges of the imaging field of view, which is important for high-precision applications [54]. Eddy currents produced in the imaging system by an alternating magnetic field can cause image artifacts and distortions or system heating, and can be reduced by pre-emphasis and shielding [55].

- **RF coil performance test** checks whether transmitting and receiving coils are functioning properly since faulty coils can lower SNR and image homogeneity. Deficient quality RF output can produce various image artifacts depending on the nature and degree of the defect [51].

- ***B_0*** **(main magnetic field) homogeneity test** determines the uniformity of the primary magnetic field over a specified volume. The homogeneity are influenced by factors such as magnet flaws, external interference, or the presence of the patient, which can be partially corrected with shim or gradient coils [51]. Low B_0 homogeneity can lead to inconsistent fat suppression, reduced signal consistency, higher wrap artifacts, image distortion, and poorer SNR in quick sequences.
- **RF power and specific absorption rate (SAR) test** checks the ability of an MRI system to adjust and monitor SAR, which is a measure of how quickly body absorbs RF energy during scanning process. High RF power levels raise tissue heating hazards, especially at higher field strengths (e.g., 3T), so SAR restrictions exist to ensure patient safety [56].

Quality control in MRI is implemented by several regulatory bodies and standardization groups, which regulate image quality, patient safety, and system performance to ensure consistent results. Key world organizations and their roles in MRI Quality Control are:

- **American College of Radiology** (ACR) ensures MRI safety, quality, and performance through established quality control protocols, accreditation, and routine monitoring by qualified personnel [57]. It is requested that ensuring diagnostic accuracy and patient safety, facilities must maintain documented quality assurance systems and undertake regular equipment evaluations.
- **American Association of Physicists in Medicine** (AAPM) is a scientific organization of medical physicists, which contributes significantly to MRI performance, particularly in the field of developing standards, safety, and quality assurance in research and clinical imaging [58]. AAPM publishes reports and guidelines for the implementation, testing and quality control in MRI, provides phantom recommendations and standards [59]. AAPM collaborates with other organizations such as ACR and FDA to create device regulations, accreditation standards and imaging policies.
- **National Electrical Manufacturers Association** (NEMA) aims to create technical standards that ensure the performance, safety, and uniformity of MRI systems from various manufacturers. NEMA develops criteria for assessing MRI system performance, such as signal-to-noise ratio, geometric distortion, and slice thickness accuracy [45].
- **Food and Drug Administration** (FDA) controls the sale and use of MRI scanners, which are designated as Class II devices due to their potential risk. These devices require pre-market clearance, and the FDA offers non-binding but strongly suggested recommendations on hardware, software, performance, safety, and site design to assist manufacturers in achieving regulatory approval [60].
- **International Electrotechnical Commission** (IEC) focuses mainly on the safety of patients and operators, as well as MRI equipment operational criteria, such as peripheral nerve stimulation and specific absorption rate [61]. IEC covers a broad range of issues and integrates some of the NEMA guidelines listed above.

Multiple international organizations establish MRI quality control standards through specific guidelines which maintain diagnostic accuracy while ensuring patient safety and equipment performance consistency:

- ACR provides strict thresholds as part of their accreditation process [51]. For instance, the geometric accuracy measurements must be within ± 2 mm of actual dimensions while percent image uniformity (PIU) must reach at least 90 % for image uniformity assessment. The regulatory standards for slice thickness accuracy require measurements to stay within ± 0.7 mm of their expected values such as 5.0 mm ± 0.7 mm. Low-contrast object detectability with ACR phantom requires at least nine spokes to be visible in its designated section and ghosting artifacts (Percent Signal Ghosting) should not exceed 2.5 %. The system must maintain its signal-to-noise ratio at levels comparable to baseline measurements. Additionally, the ACR requires that transmit gain and centre frequency remain stable because this ensures image quality consistency throughout time.
- AAPM assists to clinical standards by developing scientific protocols and technical testing procedures. The AAPM Report No. 100 [3] provides benchmark values instead of enforcing specific pass/fail thresholds: for geometric accuracy at ± 2 mm, image uniformity at ≥ 90 %, slice thickness accuracy at ± 0.7 mm, ghosting to be ≤ 2.5 % and SNR to maintain stability throughout time. AAPM guidelines suggests using phantoms to evaluate signal-to-noise ratio, geometric accuracy, image uniformity and slice thickness. The AAPM guidelines focus on

trend analysis and baseline consistency while using NEMA standards to describe test methods.

- IEC through its international standard IEC 60601-2-33 [62] establishes safety and essential performance guidelines for MRI systems. The standard establishes precise boundaries for the safety exposure of patients to electromagnetic fields, for example IEC sets Specific Absorption Rate (SAR) limits at ≤ 2.0 W/kg for whole-body exposure, ≤3.2 W/kg for the head, ≤ 10 W/kg for the torso and ≤ 20 W/kg for extremities. They also establish peripheral nerve stimulation (PNS) limits through requirements for gradient slew rate control and effective stimulus duration management to prevent nerve activation. The IEC mandates MRI systems to perform magnetic fringe field mapping while establishing a B_0 hazard zone boundary at 0.9 mT (9 Gauss) to protect patients with implanted medical devices. For acoustic safety MRI systems must provide noise exposure declarations and hearing protection when noise levels surpass established occupational safety thresholds. The IEC standards require MRI systems to have emergency shutdown functions, rapid patient evacuation procedures and MR Conditional device labelling. The IEC does not establish image quality QC thresholds, but its standards serve as essential requirements for system design, regulatory approval and safe clinical operation.

1.3.2. Phantom based MRI Quality Control

One approach to evaluate system stability and compare measurement accuracy across MRI scanners is to use a standard imaging phantom, which is an inanimate object used to characterize or calibrate imaging systems (Fig. 9) [63]. The Ad Hoc Committee was organised under the guidance of the International Society of Magnetic Resonance in Medicine (ISMRM) to develop recommendations for a system phantom that could be used to test the accuracy, stability, and comparability of MRI scanners [63]. According to Ad Hoc Committee, desired measurements are static main magnetic field B_0 (non-uniformity), RF field B_1 (non-uniformity), slice position and profile, image uniformity, geometric linearity, gradient amplitude, resolution (high-contrast detectability), SNR (low-contrast detectability), accuracy and precision in measuring proton spin relaxation times (T_1 and T_2) and proton density, also system constancy [63]. This type of system phantom could help monitoring of scanner's performance at a specific site throughout time and between different scanners, evaluate the precision of T_1 mapping and create imaging protocols that meet specific accuracy requirements, confirm scanner and protocol eligibility for clinical trials and identify the most suitable phantom manufacturing methods for future phantom development [63].

Fig. 9. Examples of MRI Phantoms: the Sun Nuclear ACR Accreditation Phantom [64] (left), used for standard image quality assessments; the Sun Nuclear SRS MR Distortion Phantom [65] (middle), designed

for evaluating geometric accuracy and distortion; and the Siemens plastic bottle phantom (right), commonly used for basic system checks and QA calibration

Recognizing the necessity for uniform phantoms, numerous organizations/initiatives have been developing MRI phantoms. These phantoms are used to characterize the physical performance of MRI systems for acceptance testing and comparison of different commercial system performance; characterize time-related changes in the physical performance of imaging systems for specific clinical protocols, and develop methods for accrediting MRI systems for clinical use [49]. Among available phantom options the ACR MRI phantom is most used and is like a golden standard in quality control of MRI systems. The American College of Radiology created this phantom to evaluate essential imaging parameters: geometric accuracy, slice thickness, spatial resolution, image intensity uniformity, ghosting artifacts and low-contrast detectability [66]. The phantom's structure contains various test objects within a uniform cylindrical body, which enables consistent, reproducible evaluation across different MRI platforms and phantom itself is a vital component of the ACR MRI accreditation program [63]. Its regular use ensures that scanners meet minimum performance standards required for clinical reliability and safety.

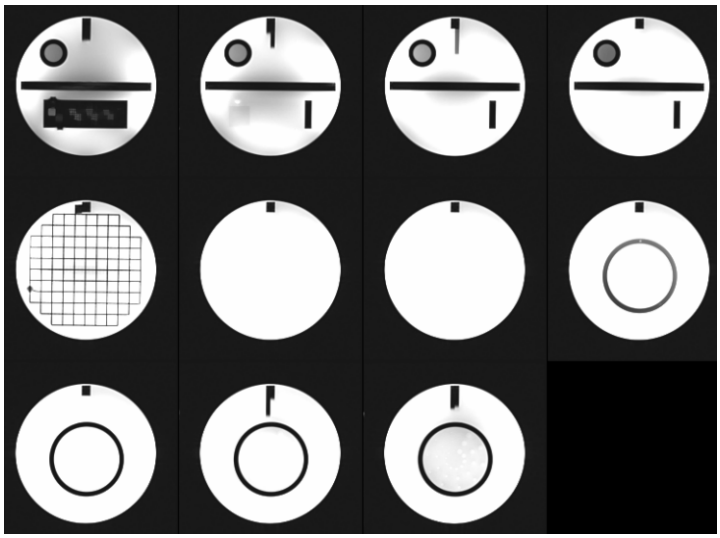

Fig. 10. MRI scans showing ACR phantom's inner structures designed to measure the geometric accuracy, high-contrast spatial resolution, slice-thickness and slice-position accuracy, image intensity uniformity, signal ghosting and low-contrast detectability [51]

The ACR phantom includes several structures to measure main image quality parameters [67]:

- **SNR, uniformity and ghosting artifacts** – these parameters are used to describe a coil's performance and monitor changes in RF coil performance. Slice without any structures is used to quantify the image SNR, uniformity and the level of artifacts being present [51]. Measuring these parameters ROI must cover at least 75 % of phantoms cross-sectional area, and appropriate air ROI must include as much background area as possible (Fig. 11).

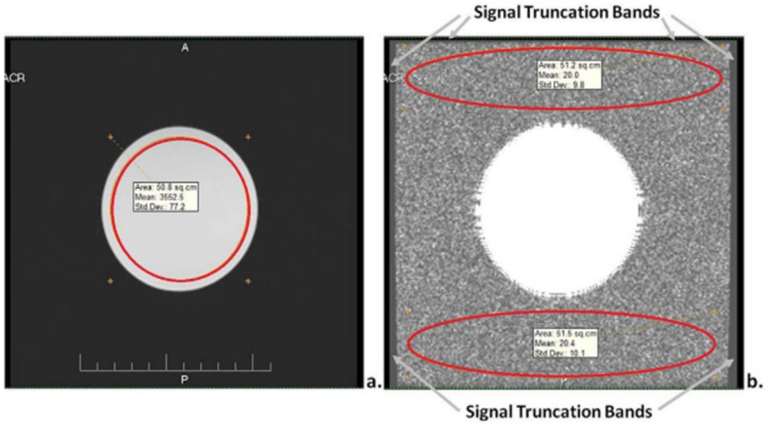

Fig. 11. ROI placements covering (a) 75 % of phantom image and (b) background area [51]

- **Geometric accuracy** is needed to verify that the image is scaled in a manner reflecting the true dimensions of the body part under investigation. Geometric accuracy is checked with the ACR MRI phantom using the sagittal localizer image from the *T_1-weighted* ACR axial series (Fig. 12). Geometric accuracy measurements using the ACR accreditation phantom are generally considered acceptable if they are within ± 2 mm of the true values [51]. **Geometry distortions** in MRI can result from miscalibrated gradients, causing one image dimension (x, y, or z) to appear stretched or compressed [51]. Gradients may drift over time and need recalibration. Distortion can also occur while using very low receiver bandwidths to boost SNR, which increases sensitivity to magnetic field inhomogeneities.

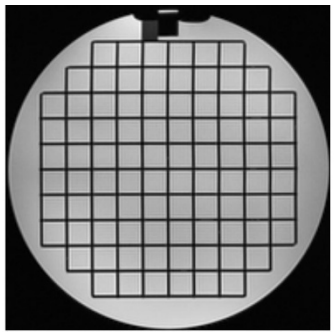

Fig. 12. MRI scan showing geometric accuracy slice [68]

- **High-Contrast Spatial Resolution** – assesses the scanner's ability to distinguish between small objects. A failure of this test indicates that for a given field of view and acquisition matrix size the scanner is not resolving fine details as effectively as a well operating scanner [51]. The *T_1-weighted* axial image of the ACR MRI phantom is used to evaluate high-contrast spatial resolution (Fig. 13). This is done by assessing the visibility of discrete fluid-filled holes within a specialized resolution insert composed of two arrays: the upper-left (UL) array, which tests resolution in the left-right direction, and the lower-right (LR) array, which tests resolution in the superior–inferior direction [51]. Each array contains staggered rows or columns of holes with precise centre-to-centre spacing, set at twice the hole diameter. The phantom contains hole pairs of different diameters from 0.7 - 1.1 mm which enables the determination of the system's spatial resolution threshold by identifying the smallest holes that can be distinguished [51]. The high-contrast spatial resolution changes because of the gradient field strength, the eddy current compensation

and the main (B_0) magnetic field homogeneity being out of calibration. Subtle decreases in spatial resolution have been reported as a result of unstable gradient amplifiers.

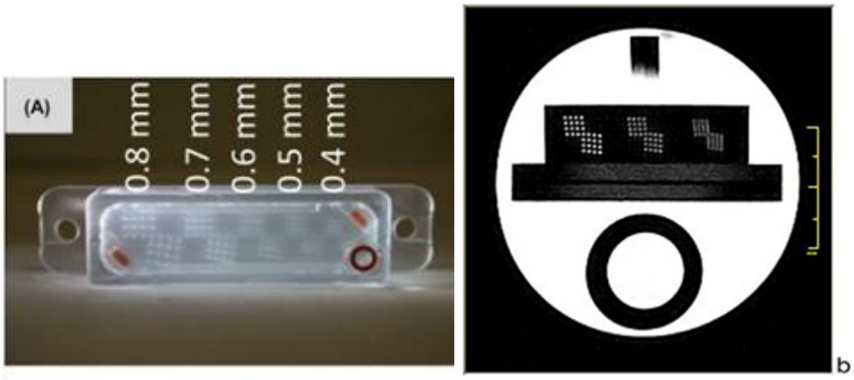

Fig. 13. An example of resolution insert (A) [63]; MRI scan showing high-contrast spatial resolution slice (B) [51]

- **Low-Contrast Detectability –** evaluates the ability of an MRI system to distinguish between structures that have small signal intensity differences from the background. The ACR MRI accreditation phantom contains low-contrast objects distributed across *T_1-weighted* multi slice series axial slices for evaluating this parameter (Fig. 14). The test objects are arranged in a radial spoke configuration which contains three identical diameter disks per spoke. The disk diameters extend from 7.0 mm to 1.5 mm through 10 clockwise steps and the contrast levels change across slices from 1.4% to 5.1% when using a 5 mm slice thickness [51]. The disks become distinguishable from the background because thin plastic inserts push solution out of their way. The observer determines the system's low-contrast resolution threshold by counting visible spokes in each slice because all disks maintain the same contrast level [51]. The evaluation does not need perfect disk shape identification but requires enough contrast to detect disks against background signal.

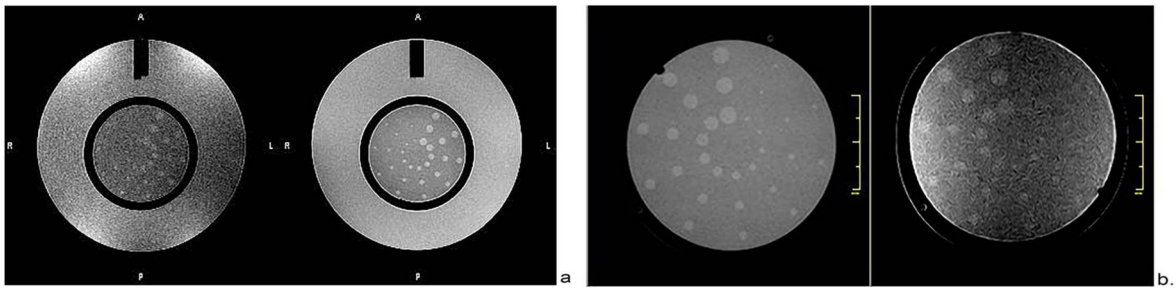

Fig. 14. MRI phantom scans of low-contrast detectability inserts: (a) large ACR phantom; (b) small ACR phantom [51]

Artifacts during the weekly, monthly or annual QC procedure may indicate a decline in MRI system performance [51]. Some artifacts obtained during quality control measurements exhibit nonspecific signs of a hardware failure. Common image distortions observed in phantom images (Fig. 15) include excessive geometric distortion, ghost images, lines or pixels with unusually high or low brightness, receiver saturation issues, unsuitable image blurring, and enhanced truncation artifacts [51]:

- Ghost images are low signal intensity representations of features in an MR image that have been moved in the phase-encoding direction. Ghosting can occur due to weak RF connections or

phantom vibrations [69]. It can be produced by instability in the measured signal from one pulse cycle to the next, which can originate in the receiver, transmitter, or gradient subsystems [51].

- Unusual bright or dark lines/pixels in MRI scans can be caused by several factors, including:
    - Bright lines can be caused by direct current (DC) offsets, incorrect 180° pulses in spin-echo sequences and RF interference. These can seem off-centre or degrade image quality depending on the readout gradient [51].
    - Zipper artifacts arise when slice excitation is imprecise, resulting in a continuous signal across phase-encoding steps, shown as a single frequency alternating line [51].
    - Bright or dark centre pixels occur by DC-offset errors, which are caused by improper scaling of low-frequency data during Fourier analysis [51].
    - Dotted lines in the phase-encoding direction are typically caused by RF interference, which suggests to check the RF shielding and examine the room equipment [51].
- Excessive filtration can result in inappropriate image blurring or truncation artifacts. The use of zero-fill interpolation or spatial resolution-enhancing filters tends to highlight truncation artifacts [51]. SNR-enhancing filters, on the other hand, tend to cause higher image blurring.
- If the RF attenuation (or gain) is not adjusted correctly during the pre-scan, signals within specific phase-encoding phases may exceed the digitizer's maximum range [69]. This causes the receiver to saturate, inhibiting proper digitization and resulting in image distortion during the inverse Fourier transform. The resulting image frequently has an unusually brilliant, smooth background that differs from random noise [51]. Similar effects can also be produced by spike signals from malfunctioning electronics.

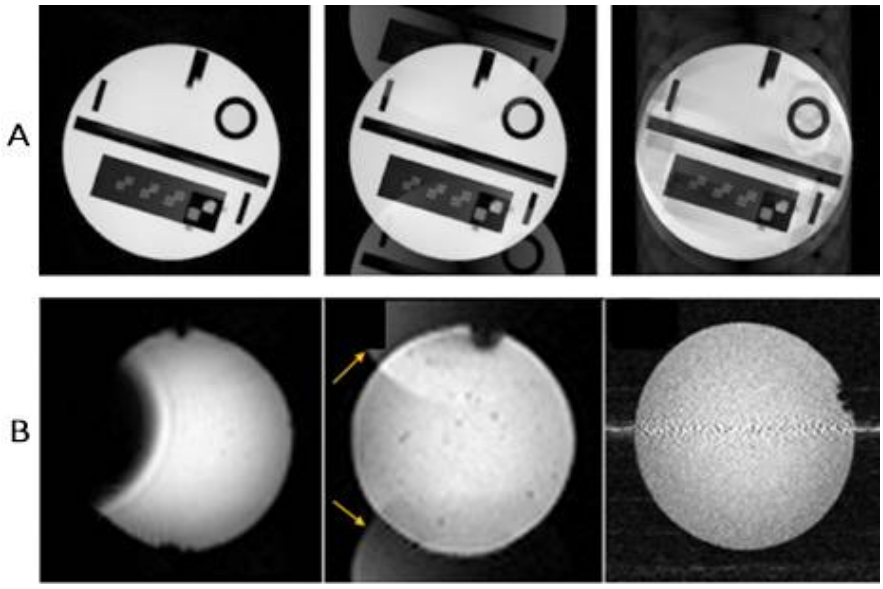

Fig. 15. (A) Phantom images with visible ghosting artifacts [70]; (B) displays various artifact types: left - susceptibility artifact; middle - ghosting artifact; right - zipper artifact [71]

As a result, any observable artifacts should be reported to the service engineer as well as the certified medical physicist or MRI scientist [51]. A trained medical physicist or MRI scientist identifies the frequency and duration of imagine artifacts for justification of study.

1.3.3. Automatization Techniques for MRI Quality Control

The manual quality control method remains effective, but it requires an extensive time and is vulnerable to operator variability. The development of automated quality control methods (Fig. 16, Fig. 17) addressed these issues with software tools that examine essential image quality characteristics such as SNR, uniformity, geometric accuracy, and ghosting artefacts.

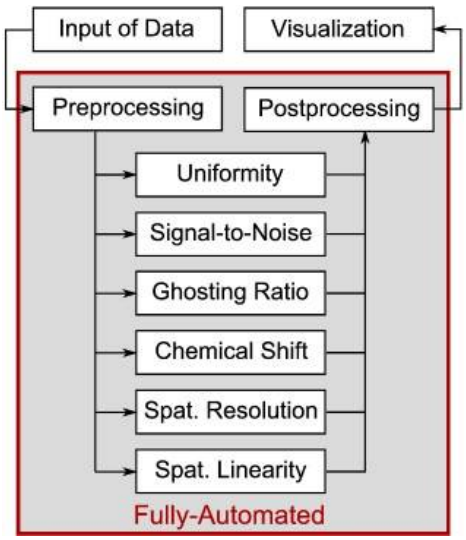

Fig. 16. Flowchart showing an example of automatization processing for phantom image dataset [67]

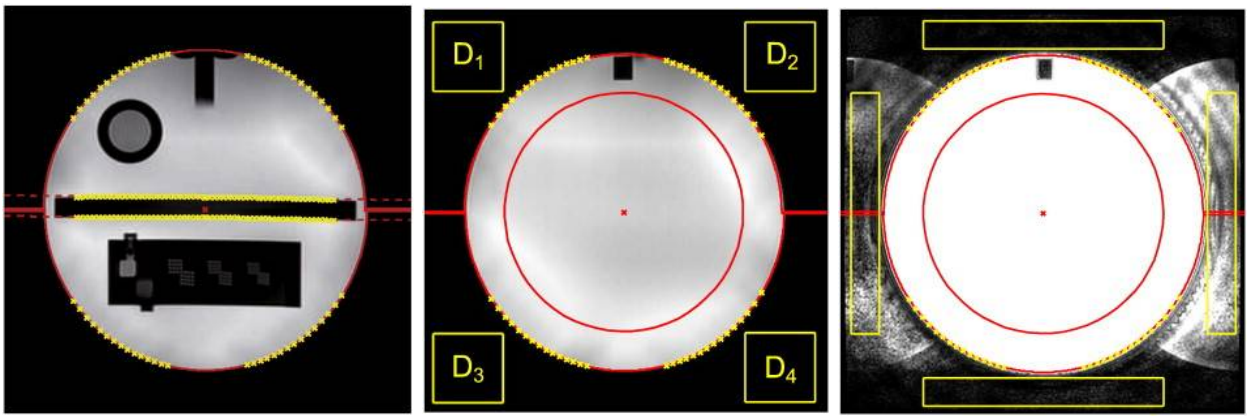

Fig. 17. An example of how automated localisation of the phantom and ROIs in the picture may look like: (left) the centre and the tilt angle determination; (middle) central and four background ROIs for SNR determination; (right) central and four elongated ROIs are used to measure the level of artifacts, providing the ghosting ratio [67]

The need for automation in quality control became evident during the late 1990s. The research by E. Gardner et al. [72] proved that automated phantom image analysis discovered minor image quality changes before trained human observers did thus demonstrating the necessity of standardized quality control procedures. The development of fully automated QC methods has led to the creation of systematic and reliable assessments for essential imaging parameters. The research conducted by M. Davids et al. [67] and J. Sun et al. [73] successfully demonstrated that automated systems provide

precise evaluations of geometric distortion, slice thickness, position accuracy, signal uniformity, ghosting, high and low-contrast resolution, chemical shift artifacts, spatial linearity and SNR. While the automated method's results were well correlated with human evaluations but automated procedures face challenges when measuring high-contrast spatial resolution as well as problems of intra-observer variability which indicates the need for further development to achieve complete autonomous QC workflows. For example in Epistatou et al. [45] study automated evaluation of four parameters were evaluated – percent signal ghosting (PSG), percent image uniformity (PIU), SNR, and SNR uniformity (SNRU). This study focussed on the reproducibility issues in MRI quality control results that emerge from irregular ROI placement on the phantom and variability in SNR calculation techniques [45]. The PSG measurement was randomised to replicate manual variability through normally distributed variations in ROI positions and dimensions that were dependent on picture resolution, pixel size, and phantom alignment. The approach allowed for statistical comparisons between automated procedures and repeated simulated measurements, which would be difficult with manual placement alone. Multiple computation approaches were utilised to evaluate SNR and SNRU, each including one or two slices from identical or closely similar sequences with varied ROI configurations. The key findings of this study were that PSG measurements are highly sensitive to background ROI placement which can be the deciding factor between passing or failing a QC test [45]. It also showed that both SNR and SNRU values vary significantly, depending on the calculation method used. This demonstrates that the AAPM, ACR, and NEMA protocols present different approaches without establishing a definitive standard because slice selection, acquisition timing and subtraction direction affect measurement results [45].

1.3.4. Impact of MRI Quality Control on Clinical Outcomes

The quality control of MRI systems determines clinical outcomes through its ability to provide reliable and consistent imaging that produce accurate diagnostic results. The systematic review of automatic QC by J. Hendriks et al. [74] demonstrates that automated and semi-automated QC methods decrease both inter and intra-rater variability and allow the early detection of image artifacts including ghosting blurring and aliasing which otherwise would affect clinical interpretation or produce wrong research and diagnostic results. Standardization methods becomes essential for large-scale or multi-site imaging studies because it enables bias reduction and cross-centre comparability [74]. Study by C. Epistatou et al. [45] demonstrates through standard phantom images that inadequate results of QC can cause image deterioration which might produce incorrect medical diagnoses and prolonged treatment times. These systems detect deviations from baseline performance while improving reproducibility which helps maintain diagnostic safety and avoids technical failures remaining unobserved [45]. The review article by K. Jhaveri [75] shows that proper QC procedures both guarantee imaging technical quality and enable precise disease detection and staging. The article explains how effective QC practices minimize the requirement for additional scans and create more streamlined clinical operations. The research by X. Yang et al. [76] demonstrates how strict quality control protocols improve MRI image quality which results in improved clinical outcomes such as earlier detection of cardiac iron overload, rectal cancer and diminished need for invasive diagnostic procedures in musculoskeletal imaging. These articles and research demonstrates that MRI QC serves as a fundamental procedure which delivers clinical confidence while protecting patient safety and enabling effective medical care.

Quality control procedures for MRI are mandatory in many countries and are typically overseen and controlled by governmental regulatory agencies. However, Lithuania currently lacks formal

regulations or national standards for MRI quality assurance and quality control. The only technical quality control conducted is an annual inspection carried out by service engineers. Because there are no regulations, there is no comprehensive record of the current status of MRI facilities in terms of commissioning protocols, routine QC testing, staff training requirements, and safety practices. In Lithuania, MRI scanners are classified as Expensive Healthcare Technology, however number of scanned patients increases each year. As MRI procedures become more accessible to patients across the country, regulations are required to ensure patient safety, increase diagnostic accuracy, optimise equipment performance and longevity, and align with international standards.

2. Instruments and methodology

2.1. MRI systems - Siemens Magnetom Skyra, Siemens Magnetom Altea and Philips Ingenia Prodiva

Parameters of 3 MRI scanners used in Lithuania and their imaging data were analysed while developing recommendations for MRI quality assurance and quality control:

- **The Siemens Magnetom Skyra (Siemens Healthcare, Germany) is a 3T MRI** (Fig. 18) scanner that provide faster and more efficient exams, as well as high-quality images for accurate diagnosis [77]. It accelerates up exams to maximize scanner utilization, standardizes and streamlines procedures. Its powerful magnet produces superior images for musculoskeletal, cardiac, neurologic, and prostate imaging [78].

- **The Siemens Magnetom Altea (Siemens Healthcare, Germany) is a 1.5T MRI** (Fig. 18) machine that provides complete assurance in productivity, repeatability, and patient satisfaction. It uses premium MRI technology and combines unique, exclusive, and revolutionary AI-powered image reconstruction technologies to fundamentally alter care delivery [79].

- **The Philips MR Ingenia Prodiva (Philips, Netherlands) is a 1.5T MRI** (Fig. 18) system that offers speed and productivity. Philips Prodiva offers improve clinical possibilities with its unique digital technology and powerful imaging solutions [80].

Fig. 18. MRI scanners used - Magnetom Skyra [77] (left), Magnetom Altea [79] (middle), Ingenia Prodiva [80] (right)

2.2. Phantoms

All mentioned MRI machines are equipped with plastic bottle phantoms. The Siemens 3T and 1.5T equipment uses various shaped bottle phantoms to simulate different human anatomies (Fig. 19). All differently shaped Siemens phantoms are filled with the paramagnetic contrast solution, composed of nickel sulphate hexahydrate ($NiSO_4 \cdot 6H_2O$) and sodium chloride (NaCl), except spherical (head) phantom which does not contain sodium chloride. The purpose of each component:

- Nickel sulphate hexahydrate ($NiSO_4 \cdot 6H_2O$) is a T_2 relaxation agent due to its paramagnetic characteristics with Ni^{2+} ions. This helps to imitate the relaxation features of soft tissues, and concentration influences the relaxation times (T_1 and T_2), making it beneficial for normalizing MRI measurements.

- Sodium chloride (NaCl) adjusts electrical conductivity to simulate human tissue. Imitates the physiological salt concentration in body fluids to ensure proper RF penetration and signal behaviour.

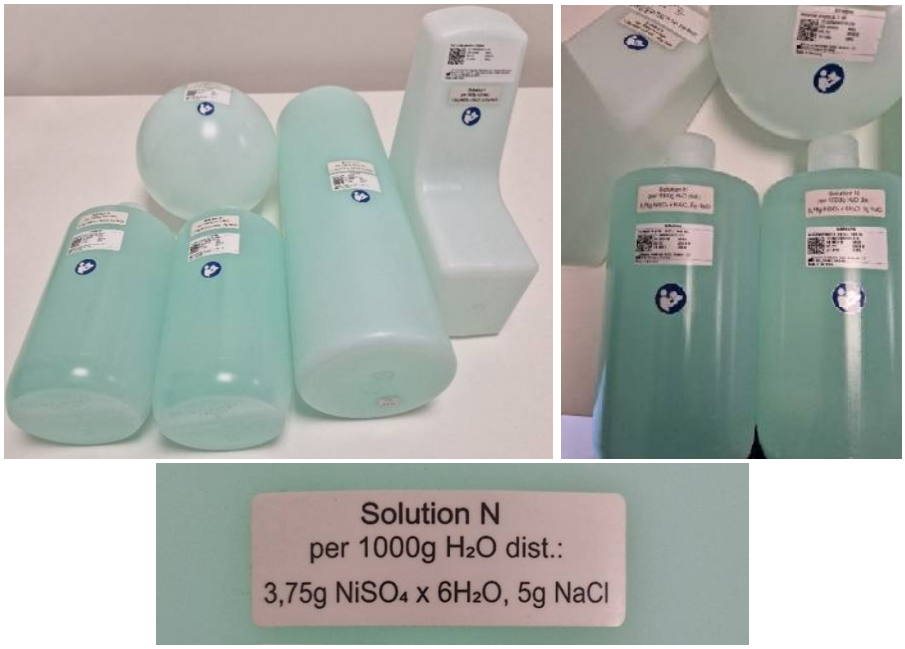

Fig. 19. Various „Siemens“ bottle phantoms filled with paramagnetic contrast solution

The Philips 1.5 T MRI machine has a single bottle phantom filled with a special „Phantom liquid 13“(composition is not disclosed) (Fig. 20).

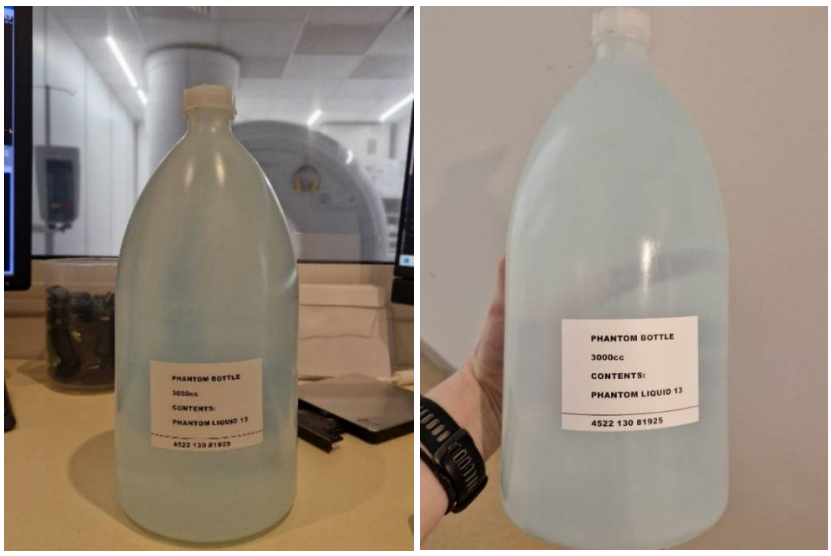

Fig. 20. „Philips“ bottle phantom

The Siemens and Philips phantoms are suitable for weekly quality control, providing accurate measurements of SNR, image uniformity (PIU) and ghosting. However, for full monthly or annual QC inspections, these phantoms are insufficient. Additional measurements, such as geometric accuracy, high-contrast spatial resolution and low-contrast detectability must be assessed using more specialized phantom such as the ACR MRI phantom.

In this work home-made spherical ACR style phantom with a 20 cm diameter was used to enable more detailed MRI quality control assessments (Fig. 21). 3D printed polylactic acid (PLA) phantom was filled with aqueous nickel chloride and sodium chloride water solution, to adjust the relaxation time of water hydrogen and to mimic tissue-like signal properties.

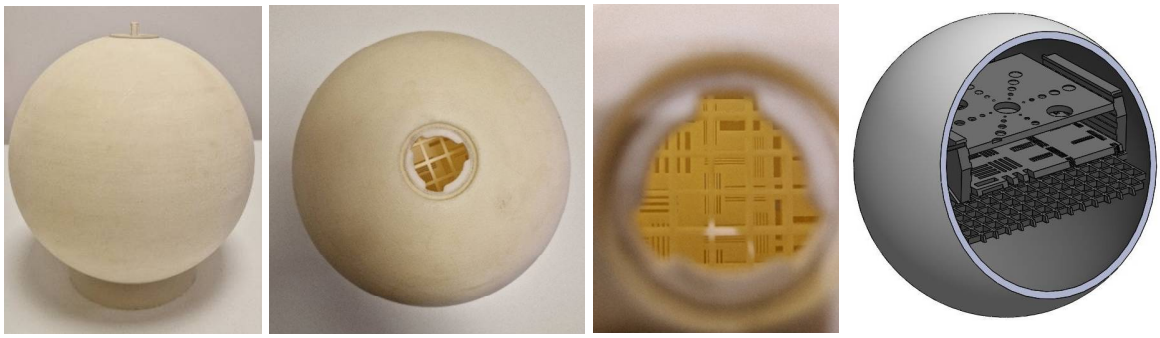

Fig. 21. Home-made ACR type phantom images and 3D Computer-aided design (CAD)

This home-made phantom consists of several dedicated test structures designed to evaluate key aspects of image quality:

- The part in the middle, which has no internal structures is used to assess image uniformity, SNR and ghosting artifacts.
- A second part has a large geometric grid for geometric distortion measurements (Fig. 22) with 160 squares of 10×10 mm each and covered by a 2 mm thick border.

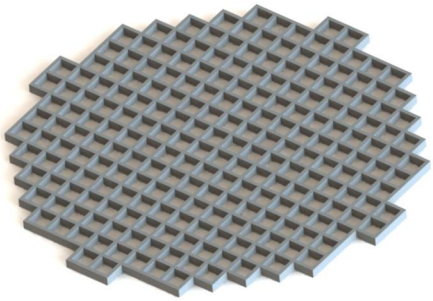

Fig. 22. Geometric distortions measurements grid with 160 squares

- Another section is for detection of low-contrast elements. It includes 30 cylindrical cavities which forms six distinct groups (Fig. 23). The five cavities in each group have the same depth but different diameters ranging from 2 - 10 mm. All these six groups demonstrate progressive contrast levels through changes in cavity depth which range from 0.25 - 2 mm.

Fig. 23. Structure for low-contrast detection, which has five same depth cavities with ranging diameters

- The last structure consists of a spatial resolution test plate contains high-contrast line-pair patterns (**Fig. 24**). A 5 mm thick plate has line-shaped cavities creating strong contrast. The resolution pattern consists of 1-6 lp/cm (line pairs per centimetre) measurements, with two parallel line-pair groups for assessing phase-encoding and frequency-encoding resolution.

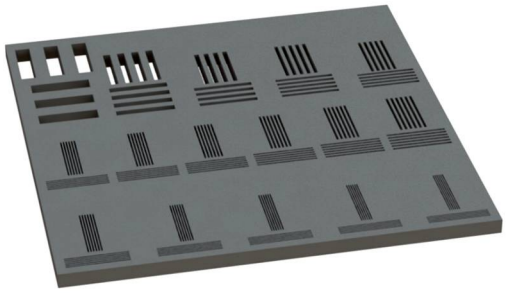

Fig. 24. Spatial resolution measurement structure with line-shaped cavities

2.3. Software

MicroDicom Viewer is a software that is primarily used for the processing and preservation of DICOM-format medical images. In this study it was used to manipulate and examine the obtained DICOM scans and measure some distances (Fig. 25).

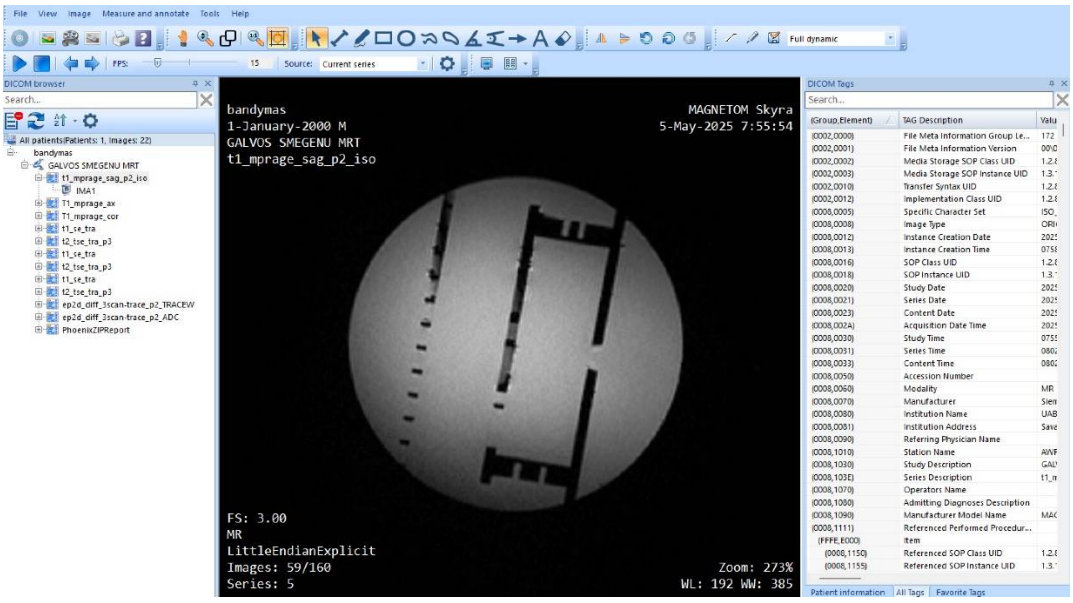

Fig. 25. The MicroDicom Viewer software interface, which displays the scans together with their DICOM data

ImageJ is open-source software for processing and evaluating scientific images. It was used with DICOM images to calculate the signal area, minimum, maximum, and mean values.

2.4. Scanning protocol parameters

Bottle and ACR phantoms were scanned using head coil as it could be seen in Fig. 26.

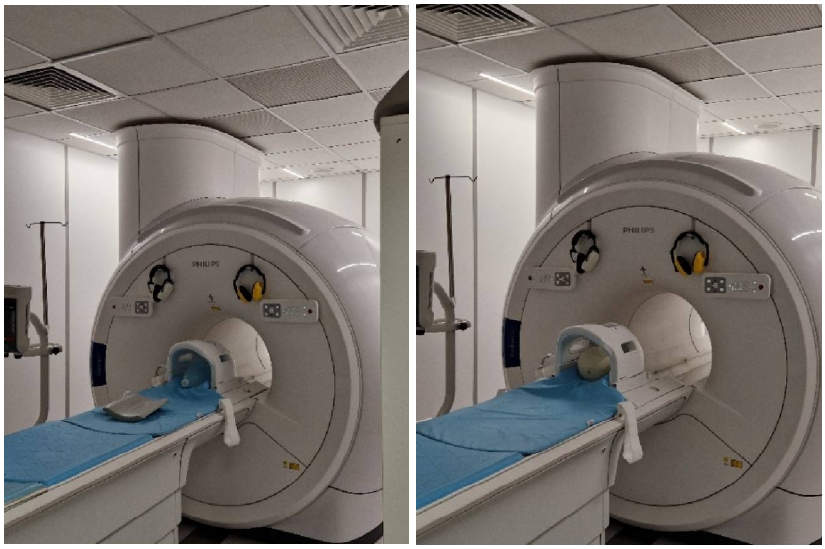

Fig. 26. Example of Philips Prodiva scanning of bottle and ACR phantoms, using head coil

Weekly bottle scans were done, for all MRI machines, using T_1, T_2 sequences and echo planar imaging (EPI). SNR and PIU was retrieved from T_1 and T_2 measurements. Parameters for weekly bottle scans (Table 1) were taken from previous MRI QC protocols, since there are no strictly defined parameters for scanning of bottle phantoms.

Table 1. Siemens MRI machine weekly (bottle phantom) scan parameters

	Siemens Magnetom Skyra (3 T)		Siemens Magnetom Altea (1.5 T)	
Series/ Pulse sequence	Axial T_1 / Spin echo	Axial T_2 / Spin echo	Axial T_1 / Spin echo	Axial T_2 / Spin echo
Coil used/ protocol	Head/ brain	Head/ brain	Head/ brain	Head/ brain
TR (ms)	600	6000	600	4000
TE (ms)	20	100	20	80
Phase encoding direction	R>>L	R>>L	R>>L	R>>L
FOV (mm)	250	250	250	250
Number of slices	27	27	25	25
Slice thickness (mm)	5	5	5	5
Spacing between slices (mm)	6.5	6.5	6.5	6.5
Matrix (phase)	256	256	256	256
Flip angle (degrees)	90	150	90	150
Bandwidth	250	250	250	250

Table 2. Philips MRI machine weekly (bottle phantom) scan parameters

	Philips Prodiva (1.5 T)	
Series/ Pulse sequence	Axial T_1 / Spin echo	Axial T_2 / Spin echo
Coil used/ protocol	Head/ brain	Head/ brain
TR (ms)	600	1000
TE (ms)	15	100
Phase encoding direction	R>>L	R>>L
FOV (mm)	250	250
Number of slices	30	30
Slice thickness (mm)	5	5
NEX	2	2
Matrix (phase)	560	560
Flip angle (degrees)	90	90
Bandwidth	250	250

The parameters used for ACR phantom scanning in this study are the official parameters for ACR accreditation (Table 3) [66, 81]. The only change was the number of slices and the slice gap. For ACR accreditation, the specified number of slices is 11. Specification of slices number is required because the ARC phantom images submitted for accreditation must include structures to appear in each slice. In this study, the main goal was to scan the ACR type phantom and evaluate obtained parameters. However due to the difficulties with capture of all required structures in their correct positions, it was decided to use 32 slices with the slice gap of 2 mm that enables covering the full length of a phantom (Fig. 27).

Table 3. American College of Radiology parameters used for ACR phantom scanning [66, 81]

Series/ Pulse sequence	Coil used/ protocol	TR (ms)	TE (ms)	FOV (mm)	Number of slices	Slice thickness (mm)	Slice Gap	Matrix (phase)
Axial T_1 / Spin echo	Head/ brain	500	20	250	32	5	2	256
Axial T_2 / Spin echo	Head/ brain	2000	80	250	32	5	2	256

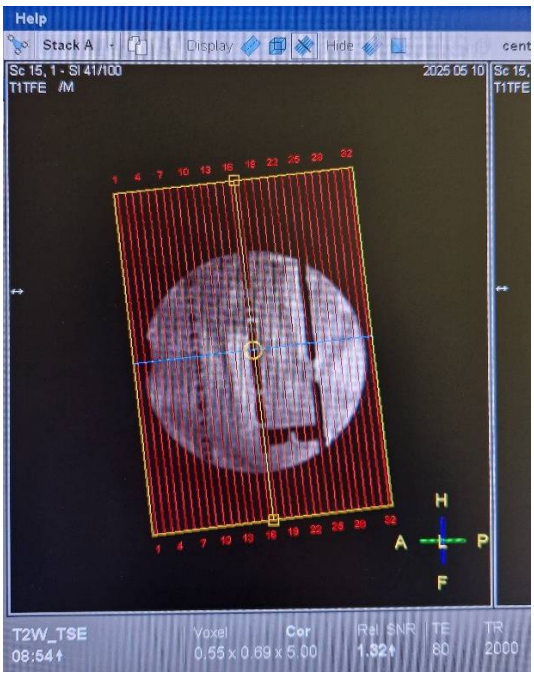

Fig. 27. ACR phantom scan planning window (Philips Prodiva) and slice direction adjustments to fit all structures

According to the ACR quality control manual [51], for signal-to-noise ratio (SNR) assessment it is crucial to evaluate the background with a low window width and appropriate level settings to prevent placing the air ROI in an area with RF leakage or values that have been zeroed by the system. Fig. 28 (right) shows a thin region of signal zeroing (signal truncation bands) around the outer border of the FOV. There is no size restriction for air ROI since it should be as large as possible to collect the best statistics on background noise signal, while excluding the signal truncation regions and signal bleed area near the phantom. The signal ROI size was selected to cover at least 75% of the phantom area, whereas the background ROI size was chosen to be as shown in Fig. 28 (left). Using ImageJ, the mean values for selected ROIs were obtained and using the Equation (2) SNR was calculated.

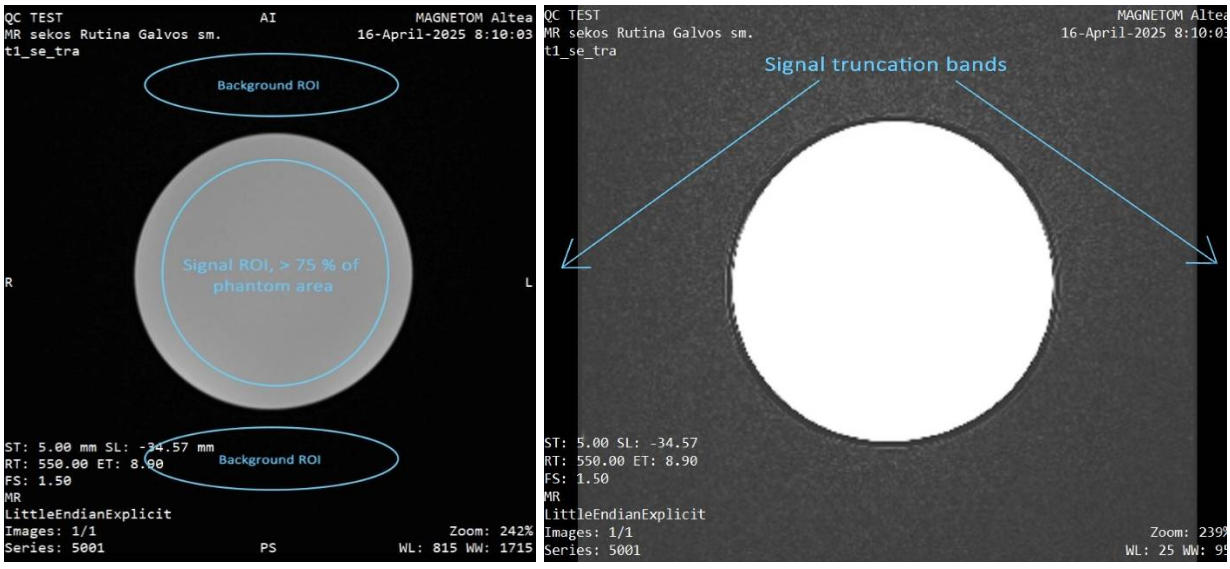

Fig. 28. Selection of signal and background ROIs for measurements (left); signal truncation bands (right)

For Percent Image Uniformity (PIU) calculations, the window width and level were modified to show the highest and lowest signal intensity regions (Fig. 29). Bright pixels have the highest signal strength,

while dark pixels have the lowest, both measured within the large ROI (at least 75% of the phantom area). The minimum and maximum ROI values (Fig. 29) were acquired using ImageJ and then were calculated using the Equation (3) .

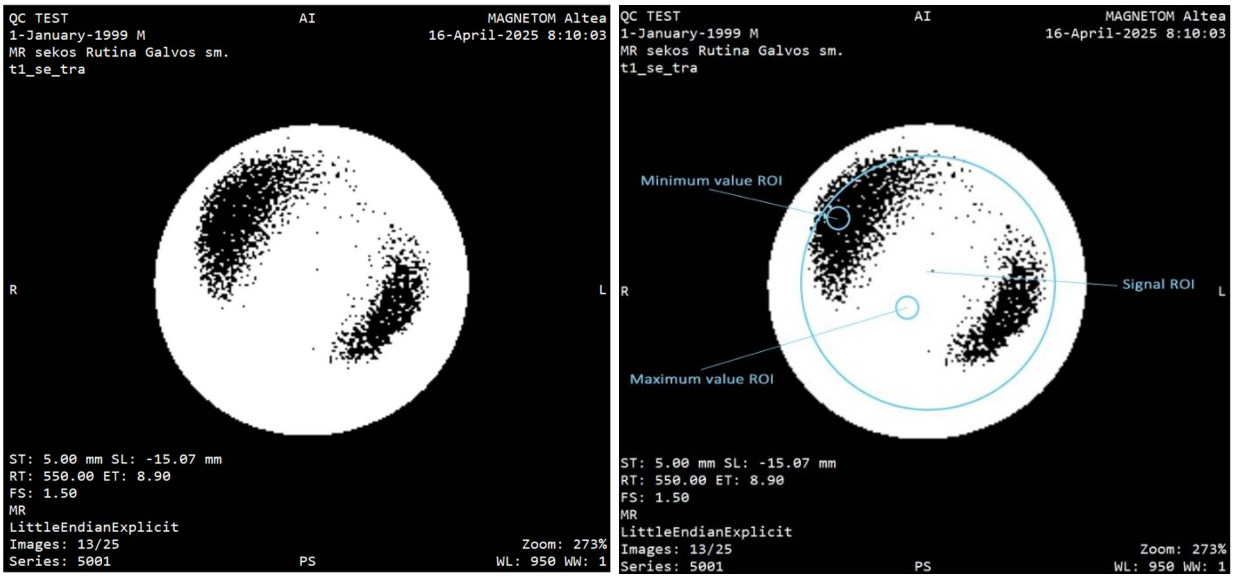

Fig. 29. Phantom image with changed windowing (left); and selected ROIs for determining maximum and minimum signal areas (right)

Geometric distortion is expressed as percent geometric distortion (PGD) and may be assessed between any two points in the field of view (Fig. 30). Equation (6) was used for PGD calculations, where the grid's real dimension is denoted by $L_{true\ dimension}$, while the dimension as measured in the image is denoted by $L_{observed\ dimension}$. The actual length of this exact ACR phantom grid was 15 cm.

$$PGD = \left(\frac{L_{true\ dimention} - L_{observed\ dimension}}{L_{true\ dimention}}\right) \cdot 100 \quad (6)$$

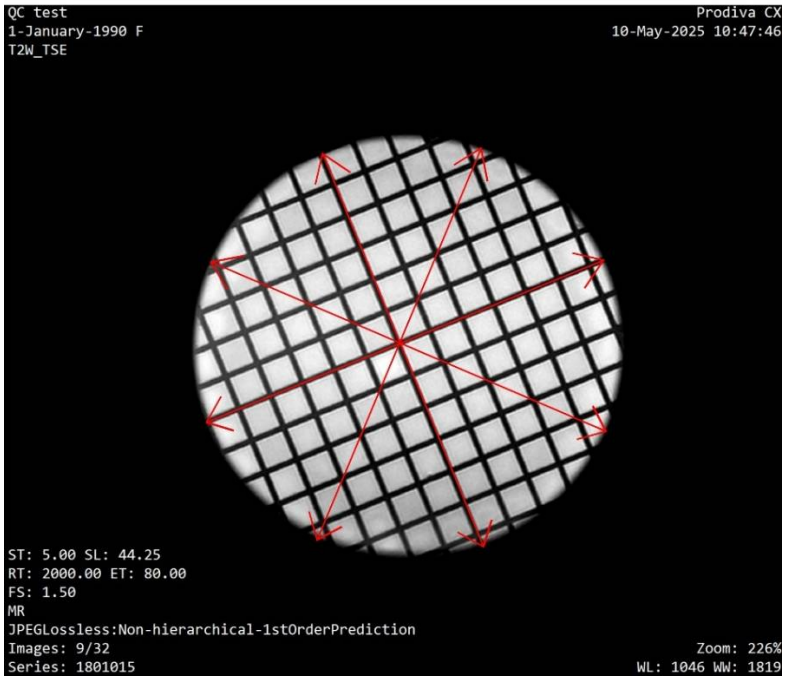

Fig. 30. Example of any two points that can be selected for PGD measurement

For Low-Contrast Detectability measurements the number of full spokes visible in the slice was counted. The ideal result for this measurement is 30 visible cavities since there are 30 cavities in total (Fig. 31) (not including the five large cavities and four smaller ones that are just used for printing and not assessment).

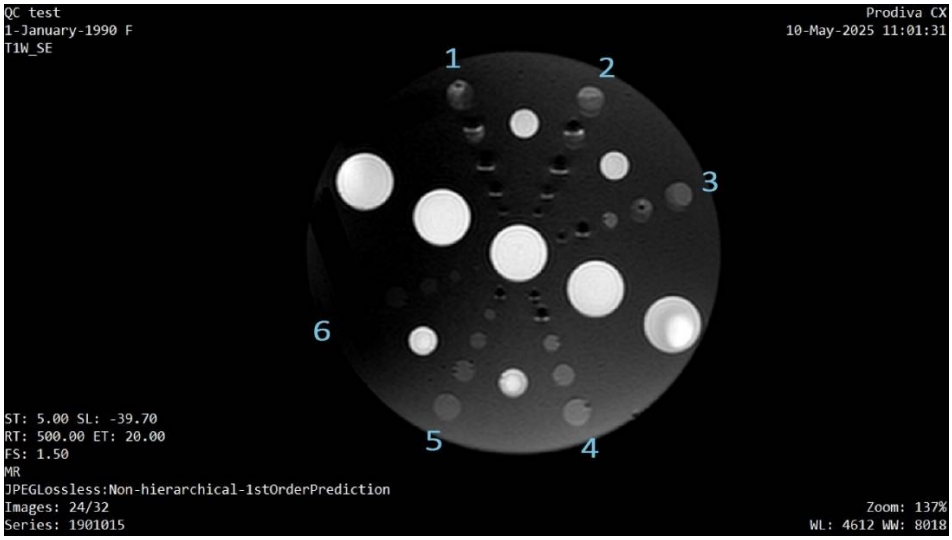

Fig. 31. Low-Contrast Detectability scan showing which group of cavities to count, 6 groups with each group having 5 cavities

High contrast resolution corresponds to a number of linear groups whose line pairs may be visually distinguished. After group 6 of line pairs (lp/cm) (Fig. 32), group 6.1 and 6.2 still has the same 6 lp/cm, but with smaller gap between them. Fig. 32 shows added numbering which corresponds to the number of line pairs in one centimetre, except for groups 6.1 and 6.2.

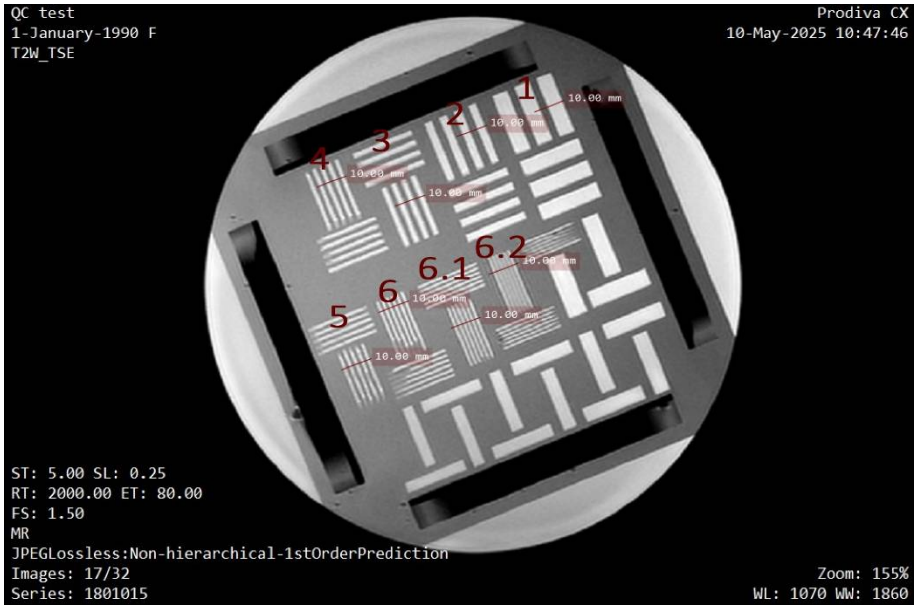

Fig. 32. High contrast resolution scan showing the number of line pairs per centimetre

3. Results and discussion

Image quality control in MRI is used for weekly and periodic routine evaluations, to optimise equipment performance and longevity, ensure patient safety and increase diagnostic quality. The recommendations for MRI quality assurance stem from the lack of formal regulations and national standards in Lithuania, so the recommendations include evaluation of key image quality parameters and establishment of baseline image quality parameter values. To achieve this, multiple scans must be performed under identical conditions across different sites. The evaluated MRI image quality parameters underwent measurement, recording and analysis with manufacturer provided and ACR style phantoms, acquisition protocols and comparison of results with ACR and AAPM guidelines.

3.1. Bottle Phantom QC – SNR, uniformity and signal ghosting

3.1.1. Signal-to-Noise Ratio

As a QC measure, SNR alone is unable to identify faults in the imaging chain. SNR issues can be caused by faulty RF coils, inadequate RF coil decoupling, pre-amplifier, receiver failures, and poor reception of external RF noise sources due to RF shield integrity issues [3]. According to AAPM SNR acceptability requirements cannot be defined in general terms since the values are system specific – RF coil, scan settings, phantom T_1 and T_2 values, etc. [3]. If provided, the SNR values should meet or exceed the values stated by the coil manufacturer. To determine the baseline, use the values obtained during installation or the values advised by the manufacturer. Table 4 and Fig. 33 presents the calculated SNR values for each scanner. The signal area (which must be greater than 75% of the phantom size) was set to 80 cm^2, whereas the background area was set to 25 cm^2 (Fig. 34). The Siemens Magnetom Skyra (3T) has the greatest SNR value for *T_1-weighted* sequence at 623.2. The 1.5T systems (Magnetom Altea and Ingenia Prodiva) had lower SNR values in T_1 (499.5 and 420.5, respectively), but still demonstrated strong image quality performance. In *T_2-weighted sequences*, all systems demonstrate a decline in SNR, which is expected given that echo times are longer and signal is inherently lower. Despite its great T_1 performance, the Skyra 3T has the lowest SNR in T_2 (165.5). The Philips Ingenia Prodiva 1.5T outperformed both Siemens systems in T_2 with SNR as 192.7, which may be due to improved signal acquisition stability or coil settings. These findings support the predicted tendency of greater SNR values in T_1 sequences, which normally increases with field strength. However, changes in scanner model, coil quality, and sequence parameters might still have an impact on final SNR results, emphasising the significance of standardising acquisition techniques when comparing systems.

Table 4. Signal-to-Noise Ratio results for T_1 and T_2 sequences across several MRI scanners

MRI Scanner	Series	Signal mean (inside phantom)	Average standard deviation (background)	Calculated SNR
Siemens Magnetom Skyra (3 T)	T_1	1290	2.1	623.2
	T_2	567	3.3	165.5
Siemens Magnetom Altea (1.5 T)	T_1	866	1.7	499.5
	T_2	511	2.9	175.9
Philips Ingenia Prodiva (1.5 T)	T_1	841	2.0	420.5
	T_2	498	2.6	192.7

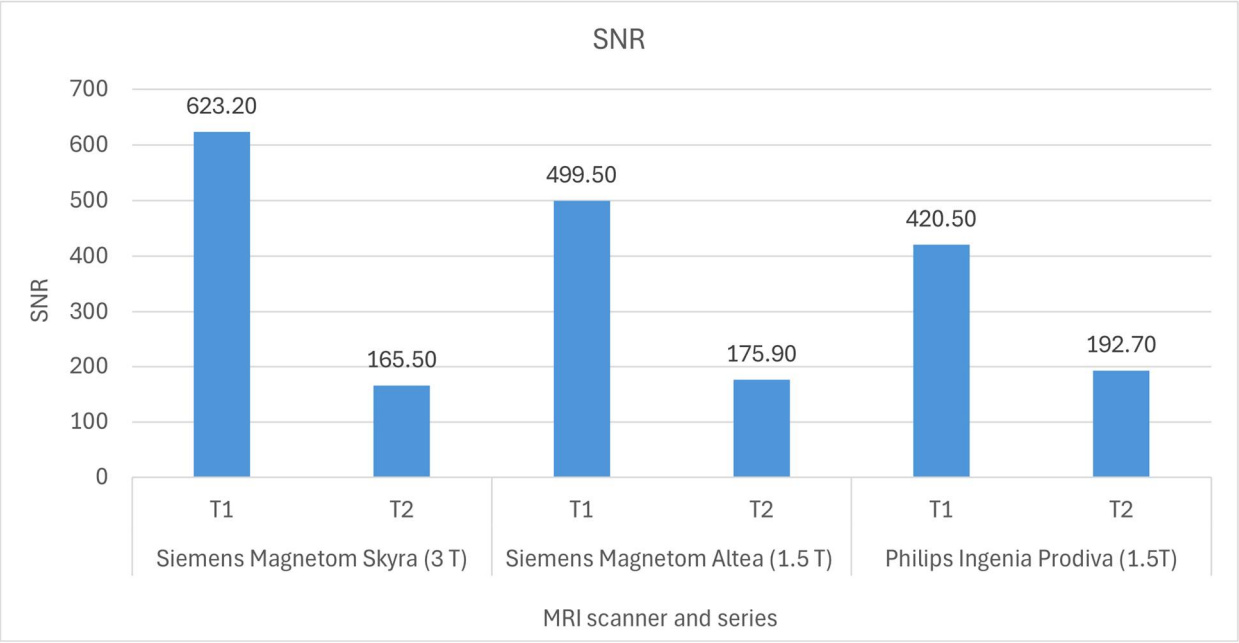

Fig. 33. Graphical representation of Signal-to-Noise Ratio results for T_1 and T_2 sequences across several MRI scanners

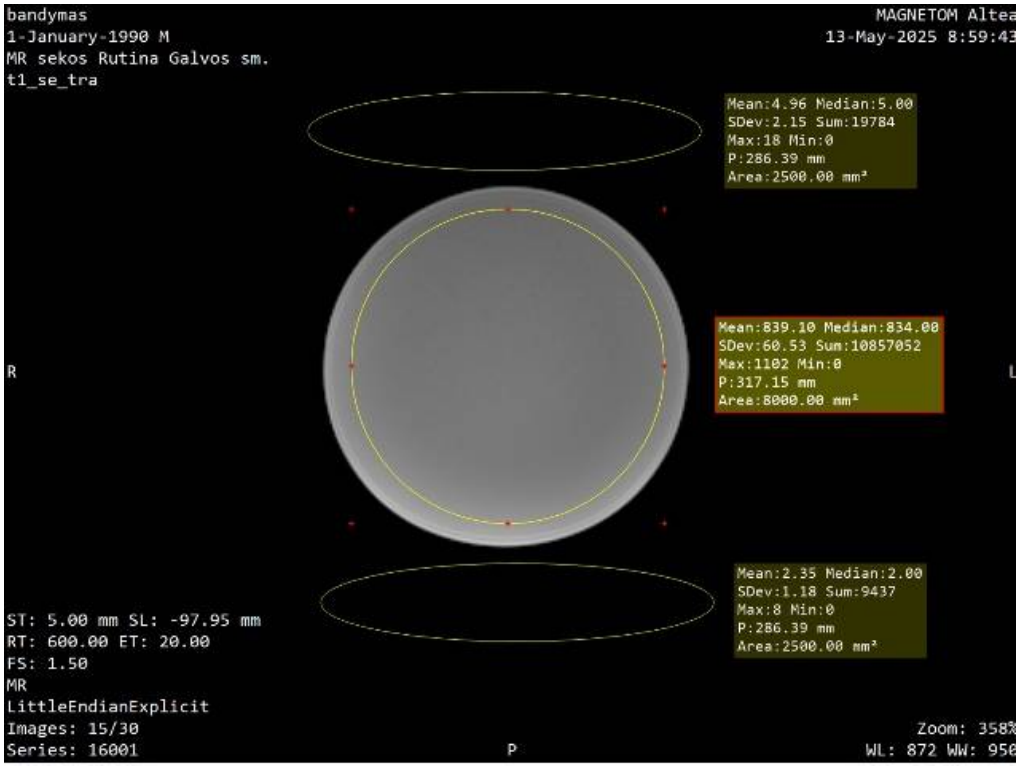

Fig. 34. Regions of interests used for signal and background measurement for SNR calculation

3.1.2. Uniformity

The MRI systems demonstrated their ability to maintain consistent signal intensity across the phantom by evaluating Percent Image Uniformity (PIU), which quantifies the homogeneity of signal distribution within a defined region of interest. According to AAPM, a volume head coil uniformity measure should be 90 % or above for scanners running at 2T or below, and less than 90 % for scanners running at field strengths higher than 2T if water-filled phantoms are being used [3]. The signal area,

same as in SNR, was adjusted to 80 cm^2, while the maximum and minimum signal pixel intensity regions were set to 1 cm^2 (Fig. 36). All three scanners uniformity results (Table 5 and Fig. 35) for the T_1 and T_2 sequences show excellent image uniformity, with all values above the 90 % threshold point established by AAPM recommendations for systems running at 2T or lower. The highest overall uniformity was reached by Philips Ingenia (1.5T) with 97.5 % in T_1 and 95.2 % in T_2, indicating the superior coil and system stability. Additionally, the Siemens Magnetom Altea (1.5 T) demonstrated similar performance in both sequences, achieving 95.6 % (T_1) and 96.3% (T_2). The Siemens Magnetom Skyra (3T) showed results slightly above 90 % – for T_1 90.7 % and for T_2 90.4 % which is expected at higher field strength, and still reflect the expected limitations, indicating the adequate uniformity and no immediate concerns. All results confirm that the systems are performing within acceptable limits, and no major uniformity issues are present. High level of uniformity among scanners points to stable coil operation and well calibrated devices for regular imaging and quality control evaluations.

Table 5. Percent image uniformity results for T_1 and T_2 sequences across several MRI scanners

MRI scanner	Series	Max signal pixel intensity	Min signal pixel intensity	Calculated PIU (%)
Siemens Magnetom Skyra (3 T)	T_1	885	835	90.7
	T_2	527	479	90.4
Siemens Magnetom Altea (1.5 T)	T_1	357	327	95.6
	T_2	602	559	96.3
Philips Ingenia Prodiva (1.5 T)	T_1	878	835	97.5
	T_2	541	485	95.2

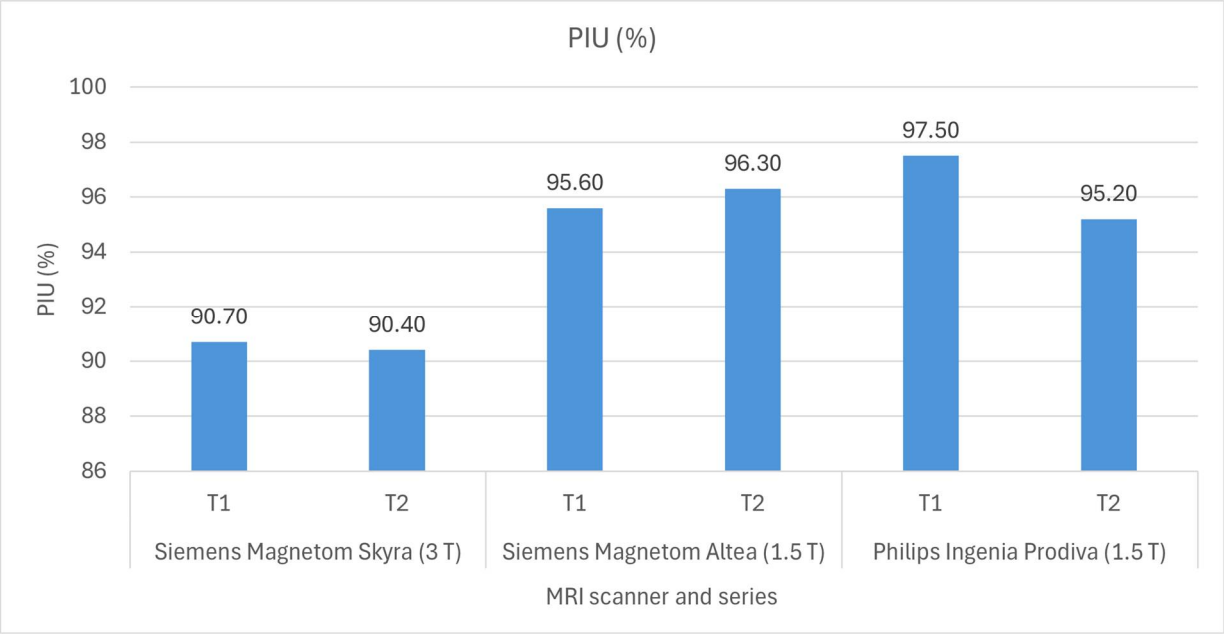

Fig. 35. Graphical representation of Percent Image Uniformity results for T_1 and T_2 sequences across several MRI scanners

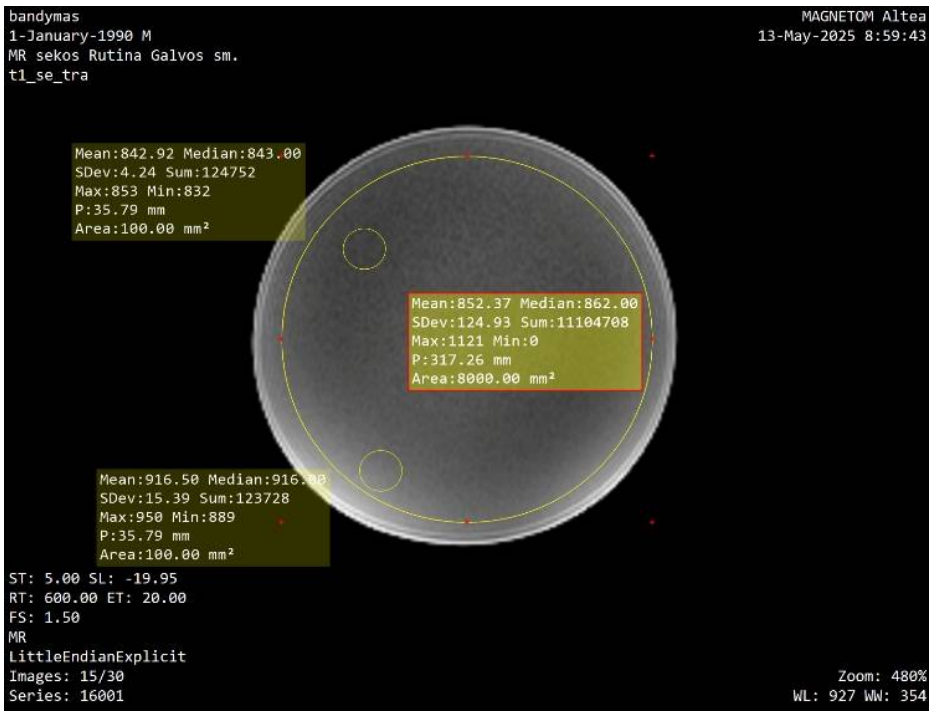

Fig. 36. Regions of interests used for maximum and minimum signal pixel intensity measurement for PIU calculation

3.2. ACR type phantom QC – geometric distortion, low-contrast object detectability and high-contrast spatial resolution

3.2.1. Geometric distortion

The geometric accuracy of the MRI systems was assessed by comparing measured phantom dimensions to known values, revealing how well spatial integrity was preserved across the field of view. Phantom images with the geometric distortion insert were measured using the ruler tool in MicroDicom Viewer. The measured diameters then were compared with the known phantom diameter of 15 cm to evaluate geometric accuracy. According to the AAPM guidelines the absolute geometric distortion should not exceed 2 % while the ACR accreditation program allows a maximum distortion of ± 2 mm when using the ACR type phantom [3]. The results (Table 6 and Fig. 37) showed that all measurements remained within these limits, with the highest deviation recorded 1.18 mm and -1.79 mm, corresponding to percentage differences of 1.12 % and -0.79 %, respectively. The highest deviation were recorded with Siemens Skyra (3T) (Fig. 40) scanner which is still in the allowed range, but shows that the higher field strengths gives more geometric distortion, unless the advanced correction methods are applied [82]. While both 1.5T systems (Fig. 38, Fig. 39) stayed below 1 mm and 0.8 % deviation. Additional measurements should be made to determine whether the reported variations are consistent as normal expected variation or fall as a systematic issue.

Table 6. Geometric distortion results for T_1 and T_2 sequences across several MRI scanners

MRI scanner	Series	Measured, mm	Difference, mm	Difference, %
Siemens Magnetom Skyra (3T)	T_1	151.79	-1.79	1.12
	T_2	148.82	1.18	-0.79
Siemens Magnetom Altea (1.5T)	T_1	151.13	-1.13	0.75
	T_2	150.71	-0.71	0.47
Philips Ingenia Prodiva (1.5T)	T_1	149.80	0.2	-0.13
	T_2	149.60	0.4	-0.27

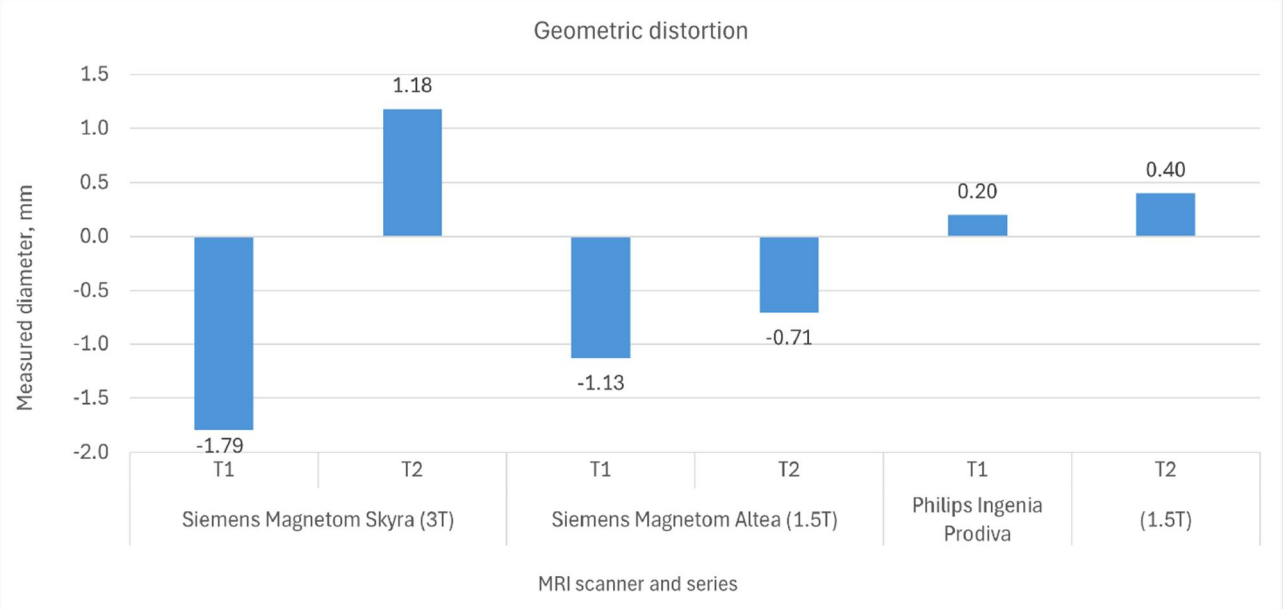

Fig. 37. Graphical representation of Geometric distortion results for T_1 and T_2 sequences across several MRI scanners

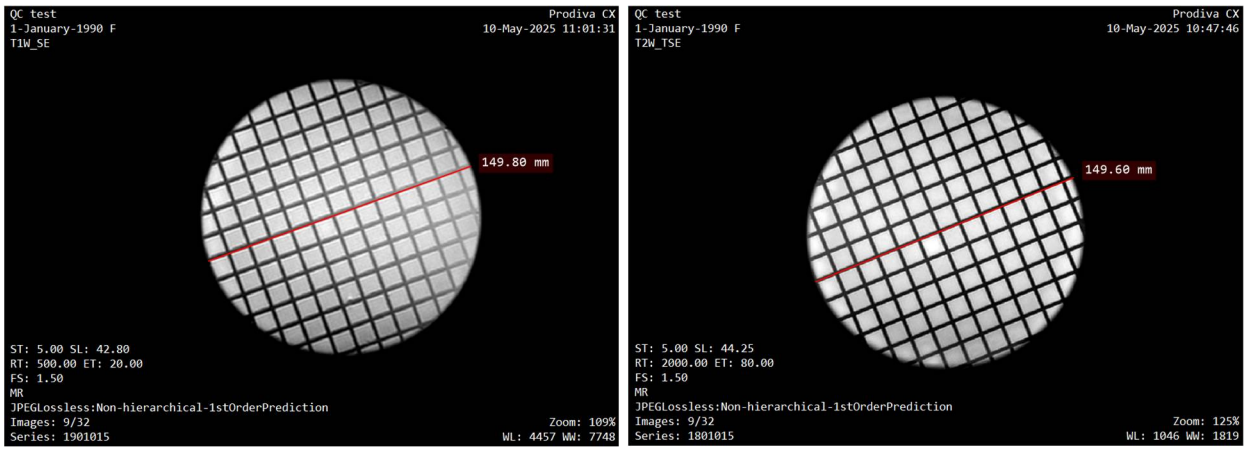

Fig. 38. Geometric accuracy evaluation on Philips Ingenia Prodiva (1.5T) system, with T_1 and T_2-*weighted* images

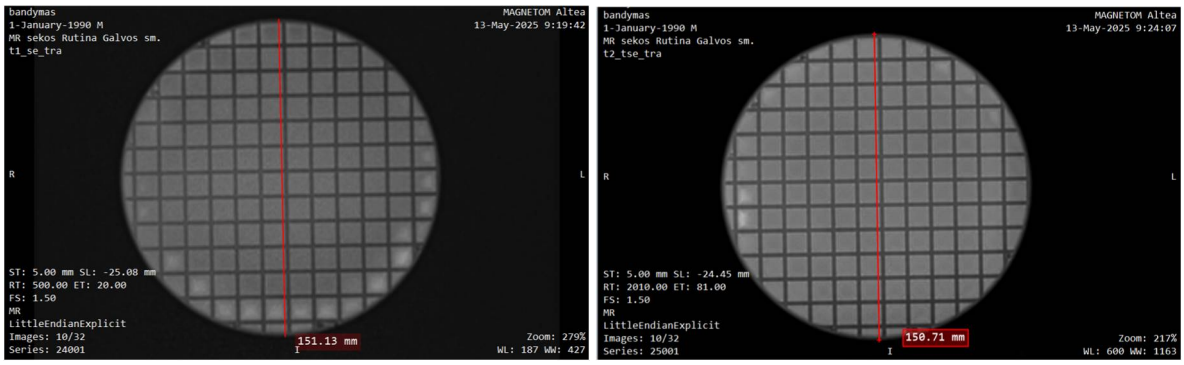

Fig. 39. Geometric accuracy evaluation on Siemens Magnetom Altea (1.5T) system, with T_1 and T_2-*weighted* images

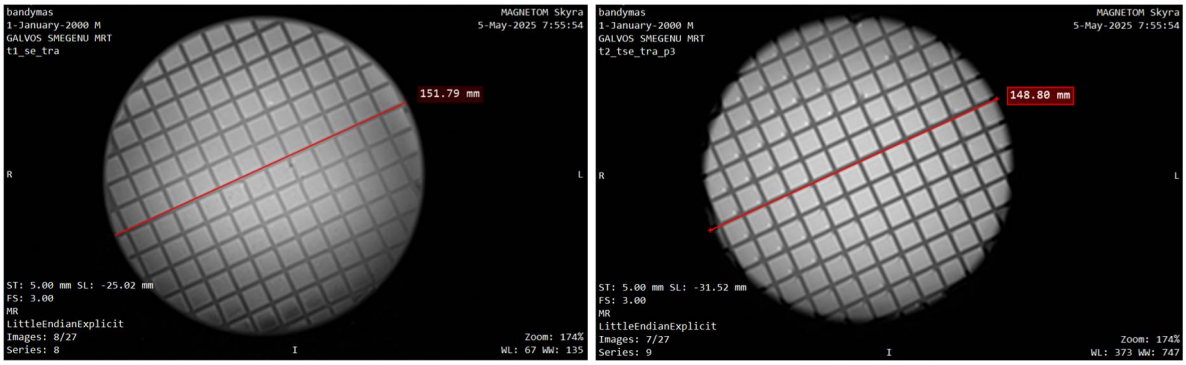

Fig. 40. Geometric accuracy evaluation on Siemens Magnetom Skyra (3T) system, with T_1 and T_2-*weighted* images

MRI diagnostic accuracy and treatment planning depend on precise geometric representation of images. Even small image geometry distortions can result in incorrect anatomical structure positioning, inaccurate lesion measurements and improper spatial registration between different scan times. The brain MRI (Fig. 41) demonstrates how geometric distortion failure produces the clinical results. Multiple axial slices show noticeable spatial warping and deformation of anatomical structures which become most pronounced at the brain periphery. The presence of such distortions in clinical imaging would both reduce diagnostic accuracy and make image-guided interventions less precise. This emphasises the importance to assess geometric distortions as a standard part of MRI quality control protocols.

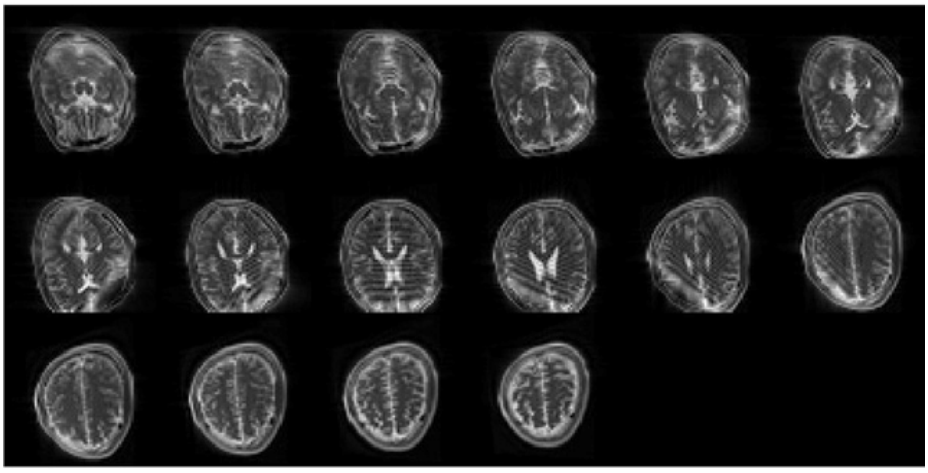

Fig. 41. An example of geometric distortion in brain MRI scans [83]

3.2.2. Low-contrast object detectability

The MRI systems demonstrated their ability to detect low-contrast objects through noise by counting the number of visible spokes. The optimal number of visible spokes should be 30, with fewer spokes visible may indicate the decrease in low-contrast detectability which could result from various factors including image noise, improper phantom positioning or limited scanner capabilities. Table 7 and Fig. 42 shows the low-contrast detectability results. The Siemens systems Magnetom Skyra (3T) (Fig. 45) and Magnetom Altea (1.5T) (Fig. 44) achieved excellent results by showing the maximum of 30 visible spokes in T_1 and T_2-*weighted* sequences. The Philips Ingenia (1.5T) (Fig. 43) system showed good performance but the T_2-*weighted* scan had 28 spokes visible which fell short of the maximum. The minor difference in results could stem from small variations in phantom positioning. The phantom used in this evaluation differs from the standard ACR phantom, so the formal ACR acceptance criteria were not applied. The results shows that all systems achieved strong performance in detecting low-contrast details.

Table 7. Low-contrast object detectability results for T_1 and T_2 sequences across several MRI scanners

MRI scanner	Series	Visible spokes	Difference
Siemens Magnetom Skyra (3T)	T_1	30	0
	T_2	30	0
Siemens Magnetom Altea (1.5T)	T_1	30	0
	T_2	30	0
Philips Ingenia Prodiva (1.5T)	T_1	30	0
	T_2	28	-2

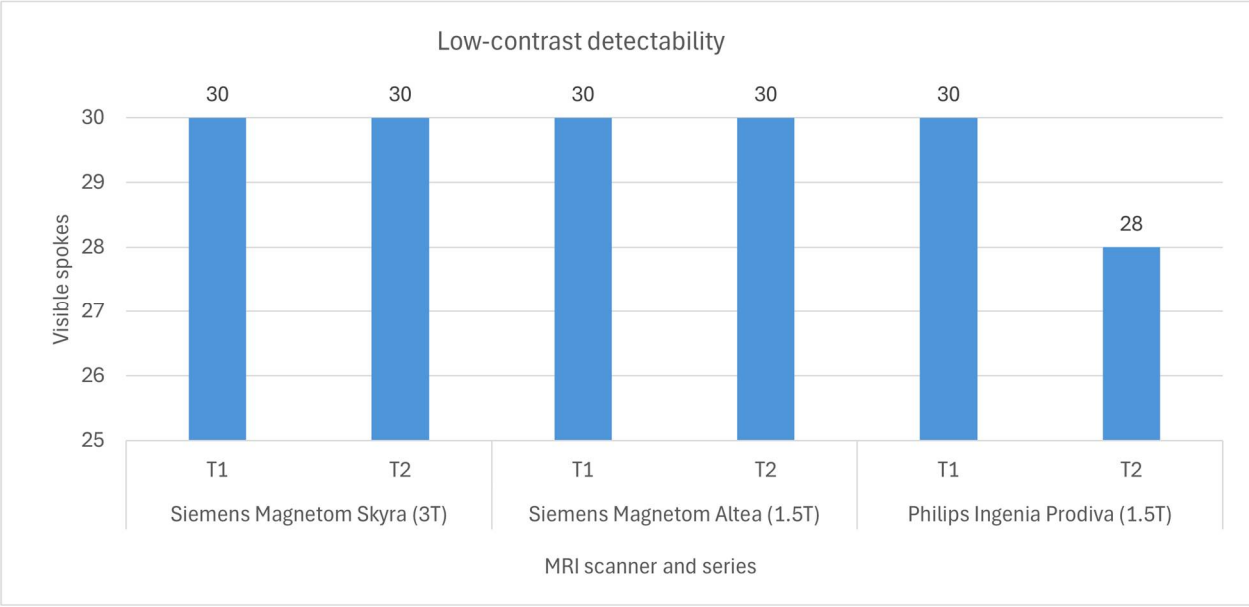

Fig. 42. Graphical representation of Low-contrast object detectability results for T_1 and T_2 sequences across several MRI scanners

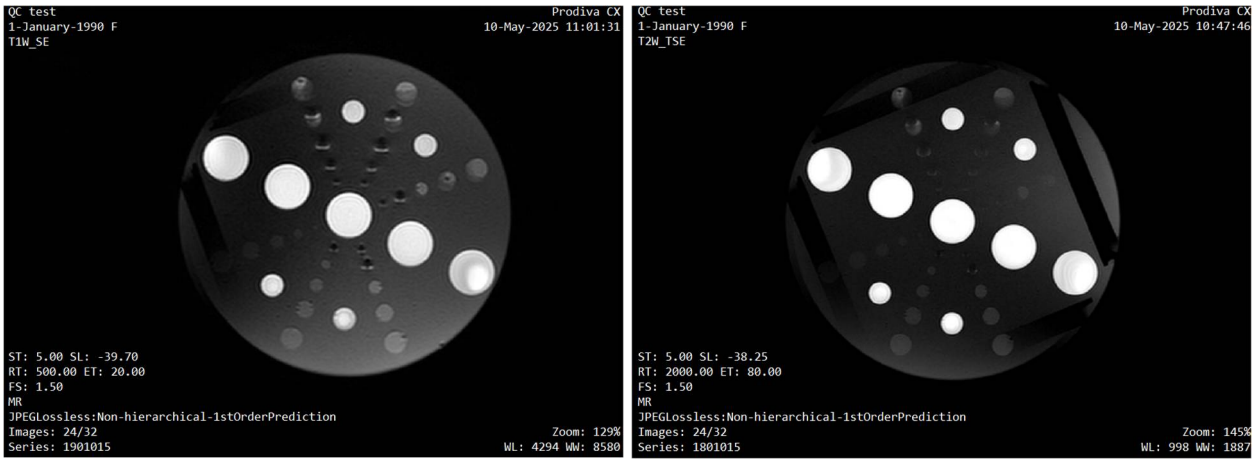

Fig. 43. Low-contrast object detectability evaluation on Philips Ingenia Prodiva (1.5T) system, with T_1 and T_2-*weighted* images

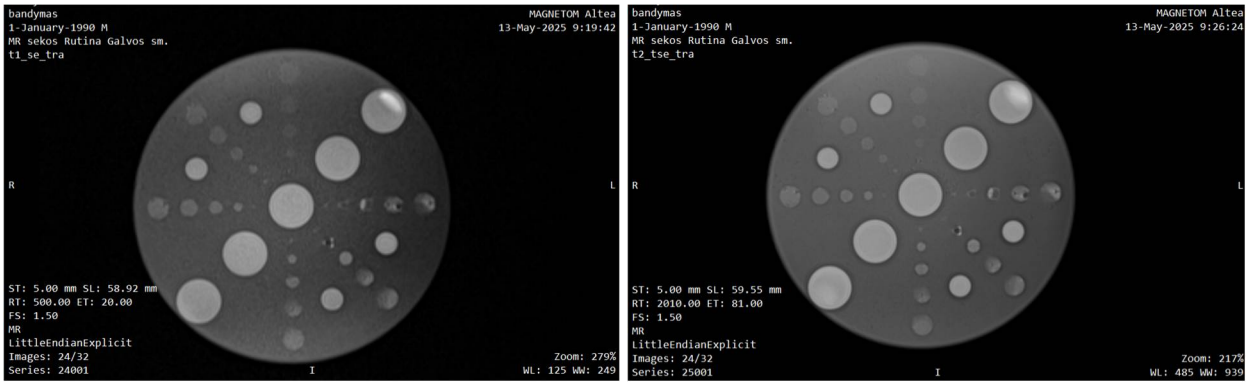

Fig. 44. Low-contrast object detectability evaluation on Siemens Magnetom Altea (1.5T) system, with T_1 and T_2-*weighted* images

Fig. 45. Low-contrast object detectability evaluation on Siemens Magnetom Skyra (3T) system, with T_1 and T_2-*weighted* images

The outcomes of poor low-contrast detectability are shown in Fig. 46 where soft tissues with similar signal intensities differentiation becomes unreliable. In Fig. 46 images from c-f shows blurring at the edges of structures, while lover group of images with region marked by green arrow shows how fine anatomical features can be lost or appear blurred when contrast detectability is insufficient. Such distortions make it difficult to accurately identify tiny lesions and clinical abnormalities.

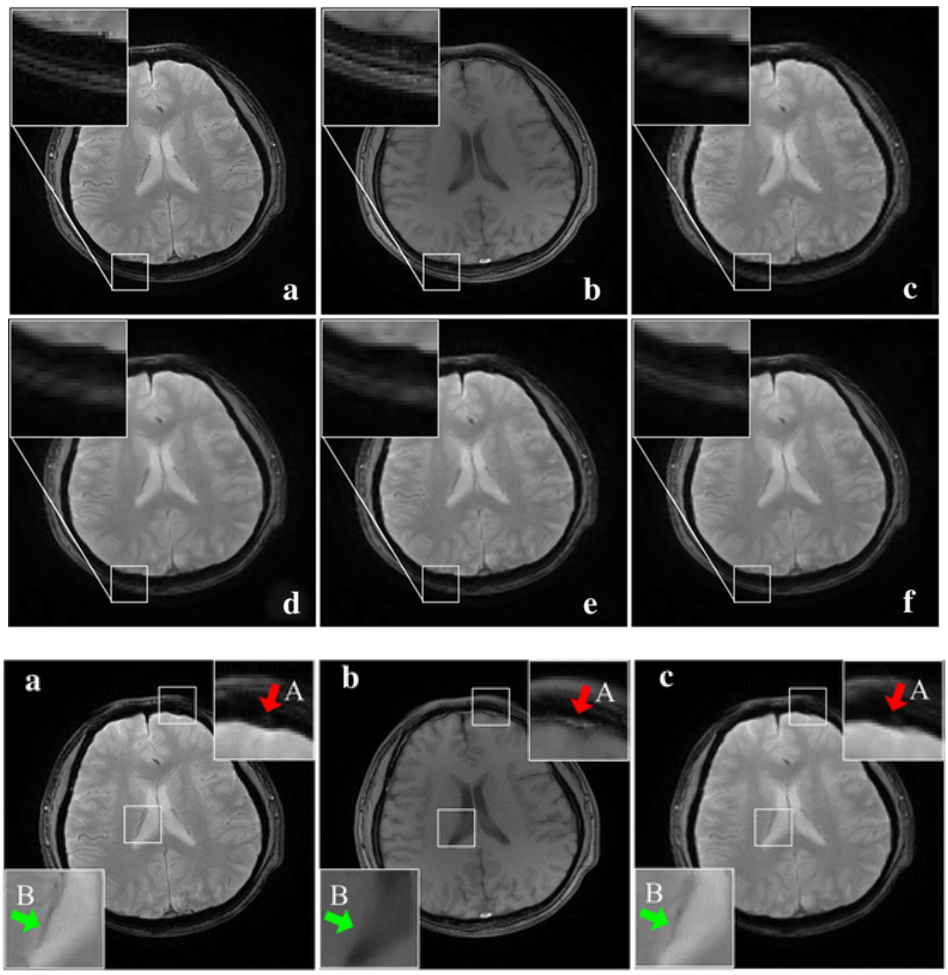

Fig. 46. MRI images showing degradation in low-contrast detectability. Upper group of images show blurring of fine anatomical details, particularly at the edges of structures, while lower images shows how low-intensity areas (marked B) become less visible for detecting tissue details and structural boundaries and how high-contrast edges become less defined (marked A) [84]

3.2.3. High-contrast spatial resolution

The evaluation of MRI scanner resolution for fine structural detail involved testing high-contrast resolution through line pair phantom assessments. The measured values (Table 8 and Fig. 47) indicate the highest group number at which line pairs remained visible (see Fig. 32 for group numbering). The AAPM acceptance criteria for high-contrast spatial resolution are based on dot phantoms (Fig. 13) yet the fundamental resolution principle can be adapted for line-pair patterns. The system demonstrates resolution of line pairs when it successfully distinguishes between consecutive black and white bars. The system needs enough pixel density to achieve this requirement just like the AAPM guideline which states that objects with one pixel width separation should be distinguishable. The highest resolution level that scanners could display is group 6.2. The 1.5T scanners Siemens Magnetom Altea (Fig. 49) and Philips Ingenia Prodiva (Fig. 48) maintained consistent high resolution performance by reaching 6.0 and 6.2 in both T_1 and T_2-*weighted* images. The 3T Siemens Magnetom Skyra scanner (Fig. 50) produced T_1-*weighted* imaging resolution that was slightly lower than the other groups (group 5) but T_2 reached group 6 which was closer to the 1.5T results. The reduced T_1 image resolution does not necessarily indicate a system fault because it could be caused by phantom

positioning errors or scanner-specific configuration. Additional repeated measurements would be necessary to determine whether this lower performance is systematic or incidental.

Table 8. High-contrast spatial resolution results for T_1 and T_2 sequences across several MRI scanners

MRI scanner	Series	Measured
Siemens Magnetom Skyra (3T)	T_1	5
	T_2	6
Siemens Magnetom Altea (1.5T)	T_1	6
	T_2	6.2
Philips Ingenia Prodiva (1.5T)	T_1	6
	T_2	6.2

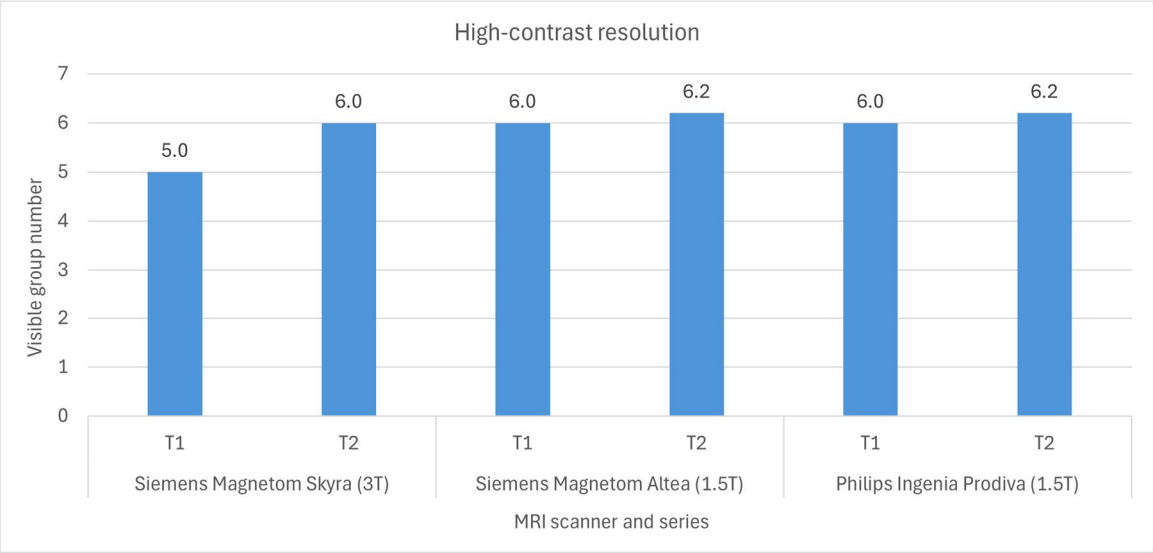

Fig. 47. Graphical representation of High-contrast spatial resolution results for T_1 and T_2 sequences across several MRI scanners

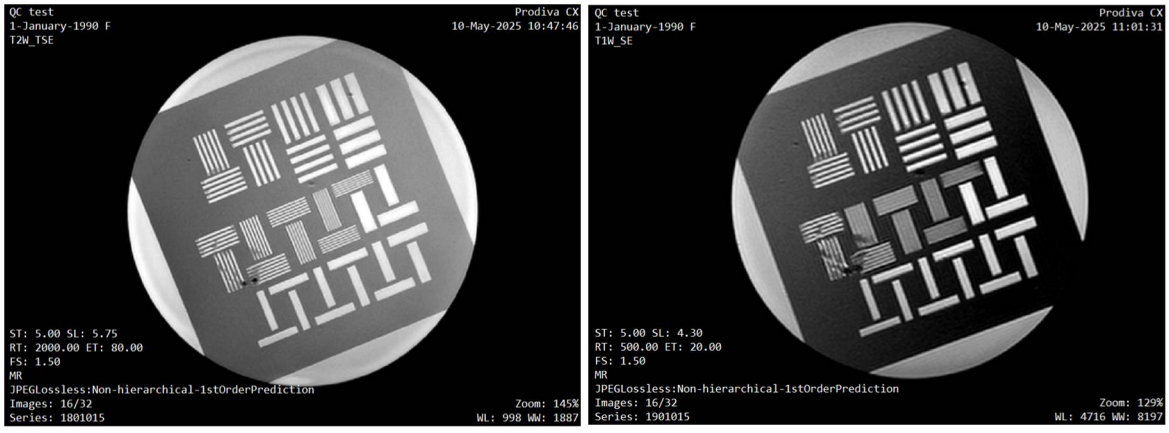

Fig. 48. High-contrast spatial resolution evaluation on Philips Ingenia Prodiva (1.5T) system, with T_1 and T_2-*weighted* images

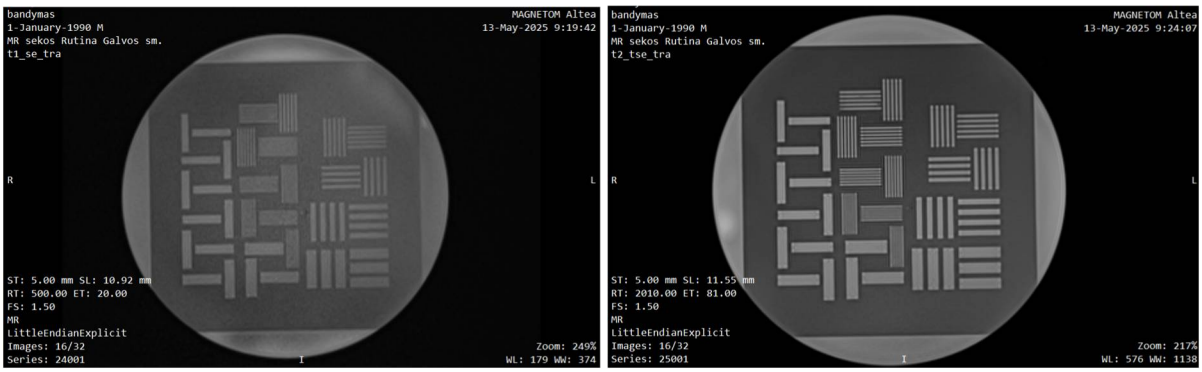

Fig. 49. High-contrast spatial resolution evaluation on Siemens Magnetom Altea (1.5T) system, with T_1 and T_2-*weighted* images

Fig. 50. High-contrast spatial resolution evaluation on Siemens Magnetom Skyra (3T) system, with T_1 and T_2-*weighted* images

High-contrast spatial resolution is an important parameter in QC because it determines the ability to clearly see fine anatomical structures and whether edges appear well defined or blurred. The clinical detection of small lesions and vascular abnormalities and cortical thinning becomes more difficult when high-contrast resolution decreases especially in areas requiring precise definition for diagnosis or surgical planning. In Fig. 51 and Fig. 52 the effects of degraded high-contrast spatial resolution is seen resulting in blurred or indistinct anatomical borders while the red arrows indicate areas where high-contrast structures should be sharply defined.

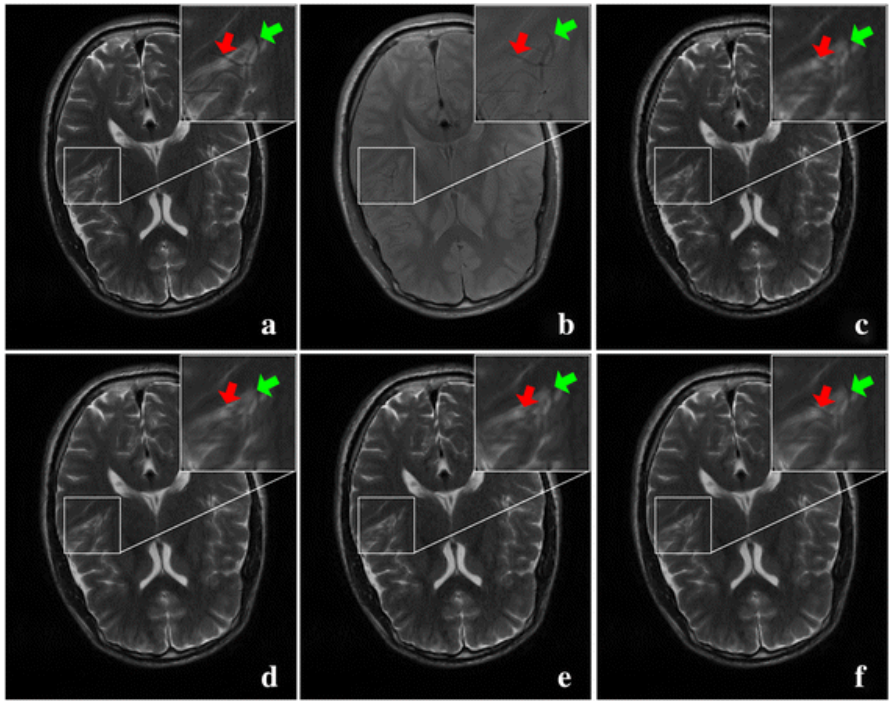

Fig. 51. Evaluation of high-contrast spatial resolution in MRI brain images. Images c-f shows degradation through the noticeable blurring and edge sharpness loss, compared to the reference images of a and b [84]

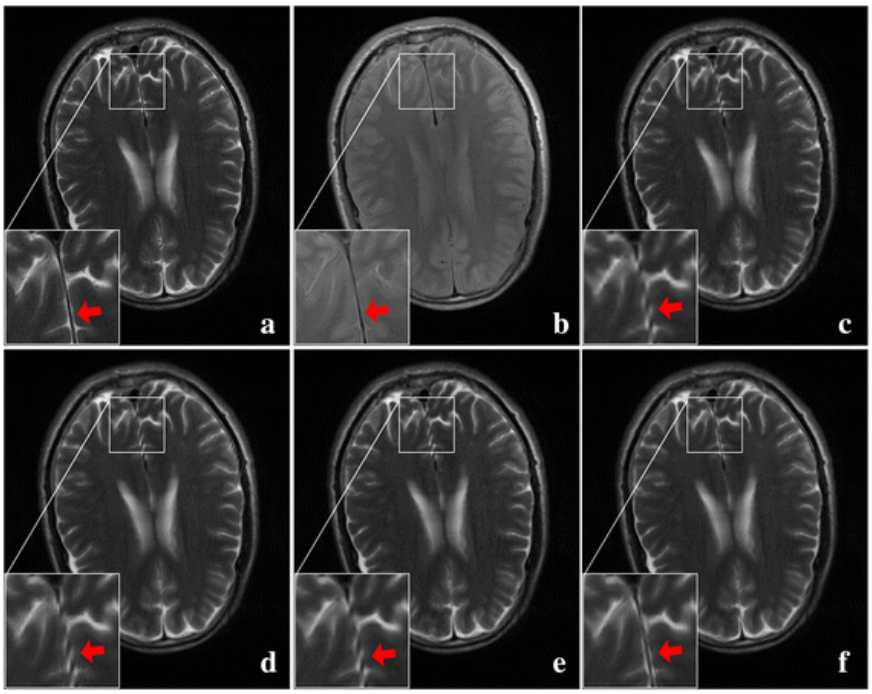

Fig. 52. Assessment of high-contrast spatial resolution using brain MRI. The reference images a (T1-weighted) and b (T2-weighted) shows high-resolution, while images c-f produce in lower high-resolution images [84]

3.3. Recommendations

According to ACR and AAPM evaluation of image data requires weekly measurements which should be performed using ACR phantom testing to assess geometric accuracy, high contrast spatial resolution, low contrast detectability, signal-to-noise ration, image uniformity and artifact evaluation.

Recommendations for MRI QC according to ACR and AAPM [3, 51]:

Staff

To minimize variability of the results and detect performance changes it is recommended that the same technologist should perform quality control (QC) measurements. The ACR recommends that a qualified medical physicist should review all QC logs at least quarterly and reassess action limits following any hardware changes or service interventions. Collaborations between radiologists, technologists, physicists and service personnel should be strengthened to ensure consistent implementation of MRI QC protocols, prompt identification of technical issues, and continuous improvement of imaging standards.

Measurements

- **Baseline**

  To establish the baseline, it is recommended to use 10 days of consistent QC results recorded using the standard forms. Due to the obtained data medical physicist may set scanner specific control limits for each parameter.
- **QC logs**

  All measurements should be recorded in a standardised QC log including the test and baseline results, if it is needed corrective actions must be done. the same procedure is recommended if any technical issues were observed. QC logs should be kept near the scanner for easy access.
- **Sequences**

  The assessment of system performance should include both T1-weighted and T2-weighted sequences for each QC parameter to reflect clinically relevant imaging protocols and to ensure a comprehensive assessment of system performance under different contrast and signal conditions. The use of both sequence types allows the identification of protocol-specific weaknesses that may only appear under certain acquisition parameters.

Performance criteria and action limits

These limits must be set and periodically reviewed by the qualified medical physicist. The guidelines and parameters for this QC were used according to ACR and AAPM:

- **SNR** – system specific, must meet or exceed manufacturer's baseline values.
- **Geometric accuracy** – within ±2 mm or 2 % (for over 25 cm FOV).
- **PIU** (Uniformity) – should be ≥ 87.5 % for 3T systems and ≥ 90 % for 1.5T.
- **Ghosting** (Percent Signal Ghosting) – ≤ 2.5%.
- **Low-contrast detectability** (using ACR provided phantom) – ≥ 9 spokes (for 1.5T) and ≥ 37 spokes (for 3T).
- **High-contrast resolution** – max line pairs visually distinguishable (to use manufacturer or ACR thresholds).
- **Corrective actions**

  When results exceed action limits the phantom re-scan should be performed and discussed the findings with the physicist and service engineer . When the repeated failure with re-scanning occurs, the software, hardware and environmental issues investigation should be mandatory performed.

Conclusions

The study aims to develop and evaluate a standardised MRI quality control (QC) methodology using phantom-based assessments on various MRI systems in Lithuania, while also validating results against international standards and highlighting the importance of structured QC in routine clinical practice.

1. QC assessments were performed using manufacturer provided bottle phantoms and an ACR-style phantom on three MRI systems: Siemens Magnetom Skyra (3T), Siemens Magnetom Altea (1.5T), and Philips Ingenia Prodiva (1.5T). The measurements included signal-to-noise ratio (SNR), percent image uniformity (PIU), geometric distortion, low-contrast object detectability, and high-contrast spatial resolution. All scanners demonstrated performance within acceptable limits. However, differences were observed based on field strength, sequence type, and device-specific configurations. For example, the Siemens Magnetom Skyra 3T had better SNR in T_1 but worse in T_2 compared to 1.5T systems, while Philips Ingenia Prodiva had the best uniformity results. These differences confirm the importance of standardized acquisition protocols for reliable cross-system comparison.
2. The results were compared to American norms from ACR and AAPM procedures, highlighting a key disparity – Lithuania lacks implemented national MRI quality control norms. While U.S. protocols offer specific thresholds and structured testing requirements, European approaches are more diverse and frequently dependent on institutional or regional regulations. The research supports the adaption of U.S. style QC structure for its clarity, reproducibility, and safety-focused integrity.
3. A practical QC protocol was developed based on American College of Radiology (ACR) and American Association of Physicists in Medicine (AAPM) guidelines for implementation in Lithuanian clinical settings. The protocol requires weekly periodic checks using phantom measurements of SNR, PIU, geometric accuracy, and resolution parameters. The establishment of baseline values during installation and the maintenance of consistent acquisition settings were found to be critical for accurate trend analysis. The protocol aims to promote routine QC integration into daily operations and to serve as a foundation for future national regulatory standards.

Acknowledgement

My sincere gratitude goes to Prof. Dr. Diana Adlienė at Kaunas University of Technology, for her support, expert advice and insightful consultations during the preparation of this master's thesis. I am also thankful to medical physicists Marius Burkanas and Mindaugas Džiugelis at the National Cancer Institute (NVI) for providing the printed phantom used in the quality control measurements. And lastly, I would like to thank the private healthcare institution InMedica for allowing to use their MRI scanners which made the practical implementation of this research possible.

List of references

1. OZBAY, Baris. Magnetic Resonance Imaging (MRI). In : *The Brain, the Nervous System, and Their Diseases: Volumes 1-3* [online]. 2014. p. 614–619. [Accessed 28 March 2025]. ISBN 9781610693387. Available from: https://www.nibib.nih.gov/science-education/science-topics/magnetic-resonance-imaging-mri
2. PEDROSA, Ivan, ALTMAN, David A., DILLMAN, Jonathan R., HOFF, Michael N., MCKINNEY, Alexander M., REEDER, Scott B., ROGG, Jeffrey M., STAFFORD, R. Jason, WEBB, James A., HERNANDEZ, Dina L. and WATSON, Robert E. *American College of Radiology Manual on MR Safety: 2024 Update and Revisions* [online]. 1 April 2025. Radiological Society of North America. [Accessed 15 May 2025]. Available from: /doi/pdf/10.1148/radiol.241405
3. JACKSON, Edward, BRONSKILL, Michael, DROST, Dick, OCH, Joseph, POOLEY, Robert, SOBOL, Wlad and CLARKE, Geoffrey. *AAPM n°100 - Acceptance Testing and Quality Assurance Procedures for Magnetic Resonance Imaging Facilities*. 2010. ISBN 9781936366026.
4. KOLLER, C. J., EATOUGH, J. P., MOUNTFORD, P. J. and FRAIN, G. A survey of MRI quality assurance programmes. *British Journal of Radiology* [online]. July 2006. Vol. 79, no. 943, p. 592–596. [Accessed 15 May 2025]. DOI 10.1259/bjr/67655734. Available from: https://pubmed.ncbi.nlm.nih.gov/16823064/
5. U.S. FOOD & DRUG ADMINISTRATION. Benefits and risks. *Canadian Mining Journal* [online]. 2023. Vol. 144, no. 5, p. 16–18. [Accessed 28 March 2025]. Available from: https://www.fda.gov/radiation-emitting-products/mri-magnetic-resonance-imaging/benefits-and-risks
6. Ultrasound vs. MRI for Diagnosis: A Comprehensive Comparison. [online]. [Accessed 28 March 2025]. Available from: https://lakezurichopenmri.com/ultrasound-vs-mri-for-diagnosis/
7. VAN BEEK, Edwin J.R., KUHL, Christiane, ANZAI, Yoshimi, DESMOND, Patricia, EHMAN, Richard L., GONG, Qiyong, GOLD, Garry, GULANI, Vikas, HALL-CRAGGS, Margaret, LEINER, Tim, LIM, C. C.Tschoyoson, PIPE, James G., REEDER, Scott, REINHOLD, Caroline, SMITS, Marion, SODICKSON, Daniel K., TEMPANY, Clare, VARGAS, H. Alberto and WANG, Meiyun. *Value of MRI in medicine: More than just another test?* [online]. 1 June 2019. John Wiley and Sons Inc. [Accessed 28 March 2025]. Available from: https://pmc.ncbi.nlm.nih.gov/articles/PMC7036752/
8. Number of MRI Scans Per Year Worldwide: Overview of global MRI utilization. [online]. [Accessed 28 March 2025]. Available from: https://about.cmrad.com/articles/number-of-mri-scans-per-year-worldwide-overview-of-global-mri-utilization
9. CERCIGNANI, Mara, DOWELL, Nicholas G. and TOFTS, Paul S. Quality Assurance: Accuracy, Precision, Controls and Phantoms. [online]. 2018. P. 33–54. [Accessed 28 March 2025]. Available from: http://www.ipem.ac.uk
10. DE GUIO, François, JOUVENT, Eric, BIESSELS, Geert Jan, BLACK, Sandra E., BRAYNE, Carol, CHEN, Christopher, CORDONNIER, Charlotte, DE LEEUW, Frank Eric, DICHGANS, Martin, DOUBAL, Fergus, DUERING, Marco, DUFOUIL, Carole, DUZEL, Emrah, FAZEKAS, Franz, HACHINSKI, Vladimir, IKRAM, M. Arfan, LINN, Jennifer, MATTHEWS, Paul M., MAZOYER, Bernard, MOK, Vincent, NORRVING, Bo, O'BRIEN, John T., PANTONI, Leonardo, ROPELE, Stefan, SACHDEV, Perminder, SCHMIDT, Reinhold, SESHADRI, Sudha, SMITH, Eric E., SPOSATO, Luciano A., STEPHAN, Blossom, SWARTZ, Richard H., TZOURIO, Christophe, VAN BUCHEM, Mark, VAN DER LUGT, Aad, VAN OOSTENBRUGGE, Robert, VERNOOIJ, Meike W., VISWANATHAN, Anand, WERRING, David, WOLLENWEBER, Frank, WARDLAW, Joanna M. and CHABRIAT, Hugues. *Reproducibility and variability of quantitative magnetic resonance imaging markers in cerebral small vessel disease* [online]. 1 August 2016. Nature Publishing

Group. [Accessed 28 March 2025]. Available from: https://pmc.ncbi.nlm.nih.gov/articles/PMC4976752/
11. JOHNS, Samantha. How NMR Works | NMR 101 | Spectroscopy | Bruker | Bruker. [online]. [Accessed 28 March 2025]. Available from: https://www.bruker.com/en/resources/library/application-notes-mr/nmr-101.html
12. MCGOWAN, Joseph C. *Basic Principles of Magnetic Resonance Imaging* [online]. 1 November 2008. Elsevier. [Accessed 25 May 2025]. Available from: https://www.sciencedirect.com/science/article/abs/pii/S1052514908000592
13. MLYNÁRIK, Vladimír. *Introduction to nuclear magnetic resonance* [online]. 15 July 2017. Academic Press. [Accessed 26 May 2025]. Available from: https://www.sciencedirect.com/science/article/pii/S0003269716300719
14. GROVER, Vijay P.B., TOGNARELLI, Joshua M., CROSSEY, Mary M.E., COX, I. Jane, TAYLOR-ROBINSON, Simon D. and MCPHAIL, Mark J.W. *Magnetic Resonance Imaging: Principles and Techniques: Lessons for Clinicians*. 1 September 2015. Elsevier.
15. PAULI, Ruth and WILSON, Martin. The Basic Principles of Magnetic Resonance Imaging. In : *Encyclopedia of Behavioral Neuroscience: Volumes 1-3, Second edition*. Elsevier, 2021. p. V1-105-V1-113. ISBN 9780128196410.
16. GIOVANNETTI, Giulio and TIBERI, Gianluigi. Radiofrequency magnetic resonance coils and communication antennas: Simulation and design strategies. *Magnetic Resonance Imaging* [online]. 1 December 2017. Vol. 44, p. 1–7. [Accessed 26 May 2025]. DOI 10.1016/j.mri.2017.07.021. Available from: https://www.sciencedirect.com/science/article/pii/S0730725X17301467
17. LEE, Mun Bae, JAHNG, Geon Ho, KIM, Hyung Joong and KWON, Oh In. High-frequency conductivity at Larmor-frequency in human brain using moving local window multilayer perceptron neural network. *PLoS ONE* [online]. 1 May 2021. Vol. 16, no. 5 May, p. e0251417. [Accessed 28 March 2025]. DOI 10.1371/journal.pone.0251417. Available from: https://pmc.ncbi.nlm.nih.gov/articles/PMC8136747/
18. T2* MRI | T2 star MRI Sequence Physics and Applications. [online]. [Accessed 28 March 2025]. Available from: https://mrimaster.com/t2-star-mri/
19. CHAVHAN, Govind B., BABYN, Paul S., THOMAS, Bejoy, SHROFF, Manohar M. and MARK HAACKE, E. Principles, techniques, and applications of T2*-based MR imaging and its special applications. *Radiographics* [online]. September 2009. Vol. 29, no. 5, p. 1433–1449. [Accessed 17 April 2025]. DOI 10.1148/rg.295095034. Available from: https://pmc.ncbi.nlm.nih.gov/articles/PMC2799958/
20. JUNG, Bernd André and WEIGEL, Matthias. Spin echo magnetic resonance imaging. *Journal of Magnetic Resonance Imaging* [online]. 1 April 2013. Vol. 37, no. 4, p. 805–817. [Accessed 28 March 2025]. DOI 10.1002/JMRI.24068. Available from: https://onlinelibrary.wiley.com/doi/full/10.1002/jmri.24068
21. MARKL, Michael and LEUPOLD, Jochen. *Gradient echo imaging* [online]. 1 June 2012. John Wiley & Sons, Ltd. [Accessed 28 March 2025]. Available from: https://onlinelibrary.wiley.com/doi/full/10.1002/jmri.23638
22. MURPHY, Andrew and BALLINGER, J. Inversion recovery sequences. In : *Radiopaedia.org*. Radiopaedia.org, 2013.
23. SARANATHAN, Manojkumar, WORTERS, Pauline W., RETTMANN, Dan W., WINEGAR, Blair and BECKER, Jennifer. *Physics for clinicians: Fluid-attenuated inversion recovery (FLAIR) and double inversion recovery (DIR) Imaging* [online]. 1 December 2017. John Wiley & Sons, Ltd. [Accessed 28 March 2025]. Available from: https://onlinelibrary.wiley.com/doi/full/10.1002/jmri.25737
24. MORATAL, David, VALLÉS-LUCH, A., MARTÍ-BONMATI, L. and BRUMMERS, M. E. k-Space tutorial: An MRI educational tool for a better understanding of k-space. *Biomedical Imaging and Intervention Journal* [online]. January 2008. Vol. 4, no. 1, p. e15. [Accessed 28 March 2025]. DOI 10.2349/biij.4.1.e15. Available from:

https://pmc.ncbi.nlm.nih.gov/articles/PMC3097694/
25. JORNADA, Tiago da Silva, MURATA, Camila Hitomi and MEDEIROS, Regina Bitelli. Influence of partial k-space filling on the quality of magnetic resonance images. *Radiologia Brasileira* [online]. 1 May 2016. Vol. 49, no. 3, p. 158–164. [Accessed 28 March 2025]. DOI 10.1590/0100-3984.2015.0028. Available from: https://pmc.ncbi.nlm.nih.gov/articles/PMC4938445/
26. GALLAGHER, Thomas A., NEMETH, Alexander J. and HACEIN-BEY, Lotfi. *An introduction to the Fourier transform: Relationship to MRI* [online]. 23 May 2008. American Roentgen Ray Society. [Accessed 28 March 2025]. Available from: https://ajronline.org/doi/10.2214/AJR.07.2874
27. Slice selection. [online]. [Accessed 28 March 2025]. Available from: https://www.radiologycafe.com/frcr-physics-notes/mr-imaging/slice-selection/
28. Frequency Encoding - Questions and Answers in MRI. [online]. [Accessed 29 March 2025]. Available from: https://mriquestions.com/frequency-encoding.html
29. MRIMASTERS. TR and TE in MRI | TR (repetition time),TE (echo time) and image contrast. [online]. [Accessed 29 March 2025]. Available from: https://mrimaster.com/tr-and-te-in-mri/
30. ELSTER, Allen. Image contrast - Questions and Answers in MRI. [online]. 2015. [Accessed 29 March 2025]. Available from: https://mriquestions.com/image-contrast-trte.html
31. HO, C. H., XIAO, L., KWOK, K. Y., YANG, S., FUNG, B. W.H., YU, K. C.H., CHONG, W. H., YEUNG, T. W. and LI, A. Common Artifacts in Magnetic Resonance Imaging: A Pictorial Essay. *Hong Kong Journal of Radiology*. 1 March 2023. Vol. 26, no. 1, p. 58–65. DOI 10.12809/hkjr2317476.
32. MCCONNELL, J. Fraser. MRI ARTIFACTS. In : *Diagnostic MRI in Dogs and Cats* [online]. Radiopaedia.org, 2018. p. 70–87. [Accessed 29 March 2025]. ISBN 9781498737715. Available from: https://radiopaedia.org/articles/16585
33. SERAI, Suraj D., HO, Mai Lan, ARTUNDUAGA, Maddy, CHAN, Sherwin S. and CHAVHAN, Govind B. *Components of a magnetic resonance imaging system and their relationship to safety and image quality* [online]. 1 May 2021. Pediatr Radiol. [Accessed 29 March 2025]. Available from: https://pubmed.ncbi.nlm.nih.gov/33871725/
34. GRUBER, Bernhard, FROELING, Martijn, LEINER, Tim and KLOMP, Dennis W.J. *RF coils: A practical guide for nonphysicists* [online]. 1 September 2018. John Wiley and Sons Inc. [Accessed 29 March 2025]. Available from: https://pmc.ncbi.nlm.nih.gov/articles/PMC6175221/
35. YOUSAF, Tayyabah, DERVENOULAS, George and POLITIS, Marios. Advances in MRI Methodology. In : *International Review of Neurobiology* [online]. Int Rev Neurobiol, 2018. p. 31–76. [Accessed 29 March 2025]. ISBN 9780128154182. Available from: https://pubmed.ncbi.nlm.nih.gov/30314602/
36. REPORT, Mid-semester and BWIG, Luisa Meyer. MRI Gradient Coils. [online]. 2018. [Accessed 29 March 2025]. Available from: https://info.atlantisworldwide.com/blog/mri-gradient-coils-101
37. HOOGENRAAD, Frank, GEERTS-OSSEVOORT, Liesbeth and HARVEY, Paul. *Accuracy, power and endurance in MRI A modern perspective on gradient system performance*. 2022.
38. KAWAHARA, Daisuke and NAGATA, Yasushi. T1-weighted and T2-weighted MRI image synthesis with convolutional generative adversarial networks. *Reports of Practical Oncology and Radiotherapy* [online]. 2021. Vol. 26, no. 1, p. 35–42. [Accessed 30 March 2025]. DOI 10.5603/RPOR.a2021.0005. Available from: https://pmc.ncbi.nlm.nih.gov/articles/PMC8086713/
39. KATES, Robin, ATKINSON, Dennis and BRANT-ZAWADZKI, Michael. *Fluid-attenuated inversion recovery (FLAIR): Clinical prospectus of current and future applications* [online]. 1996. [Accessed 30 March 2025]. Available from: https://pubmed.ncbi.nlm.nih.gov/9402679/
40. BALIYAN, Vinit, DAS, Chandan J, SHARMA, Raju and GUPTA, Arun Kumar. Diffusion

weighted imaging: Technique and applications. *World Journal of Radiology* [online]. 2016. Vol. 8, no. 9, p. 785. [Accessed 30 March 2025]. DOI 10.4329/wjr.v8.i9.785. Available from: https://pmc.ncbi.nlm.nih.gov/articles/PMC5039674/

41. THE JOHNS HOPKINS UNIVERSITY, THE JOHNS HOPKINS HOSPITAL and THE JOHNS HOPKINS HEALTH SYSTEM. Magnetic Resonance Angiography (MRA) | Johns Hopkins Medicine. [online]. 2021. [Accessed 30 March 2025]. Available from: https://www.hopkinsmedicine.org/health/treatment-tests-and-therapies/magnetic-resonance-angiography-mra
42. GLOVER, Gary H. *Overview of functional magnetic resonance imaging* [online]. April 2011. [Accessed 30 March 2025]. Available from: https://pmc.ncbi.nlm.nih.gov/articles/PMC3073717/
43. VARGAS, M. I., DELATTRE, B. M.A., BOTO, J., GARIANI, J., DHOUIB, A., FITSIORI, A. and DIETEMANN, J. L. *Advanced magnetic resonance imaging (MRI) techniques of the spine and spinal cord in children and adults* [online]. 1 August 2018. Springer Verlag. [Accessed 30 March 2025]. Available from: https://pmc.ncbi.nlm.nih.gov/articles/PMC6108966/
44. YOO, Roh Eul. Diffusion Tensor Imaging. In : *Surgery of Spinal Cord Tumors Based on Anatomy: An Approach Based on Anatomic Compartmentalization* [online]. StatPearls Publishing, 2021. p. 147–151. [Accessed 30 March 2025]. ISBN 9789811577710. Available from: https://www.ncbi.nlm.nih.gov/books/NBK537361/
45. EPISTATOU, Angeliki C., TSALAFOUTAS, Ioannis A. and DELIBASIS, Konstantinos K. An Automated Method for Quality Control in MRI Systems: Methods and Considerations. *Journal of Imaging* [online]. 1 October 2020. Vol. 6, no. 10, p. 111. [Accessed 20 April 2025]. DOI 10.3390/jimaging6100111. Available from: https://pmc.ncbi.nlm.nih.gov/articles/PMC8321175/
46. PROVINS, Céline, MACNICOL, Eilidh, SEELEY, Saren H., HAGMANN, Patric and ESTEBAN, Oscar. Quality control in functional MRI studies with MRIQC and fMRIPrep. *Frontiers in Neuroimaging* [online]. 12 January 2023. Vol. 1, p. 1073734. [Accessed 20 April 2025]. DOI 10.3389/fnimg.2022.1073734. Available from: https://pmc.ncbi.nlm.nih.gov/articles/PMC10406249/
47. BARNES, Anna, ALONZI, Roberto, BLACKLEDGE, Matthew, CHARLES-EDWARDS, Geoff, COLLINS, David J., COOK, Gary, COUTTS, Glynn, GOH, Vicky, GRAVES, Martin, KELLY, Charles, KOH, Dow Mu, MCCALLUM, Hazel, MIQUEL, Marc E., O'CONNOR, James, PADHANI, Anwar, PEARSON, Rachel, PRIEST, Andrew, ROCKALL, Andrea, STIRLING, James, TAYLOR, Stuart, TUNARIU, Nina, VAN DER MEULEN, Jan, WALLS, Darren, WINFIELD, Jessica and PUNWANI, Shonit. Guidelines & recommendations: UK quantitative WB-DWI technical workgroup: Consensus meeting recommendations on optimisation, quality control, processing and analysis of quantitative whole-body diffusion-weighted imaging for cancer. *British Journal of Radiology* [online]. 1 January 2018. Vol. 91, no. 1081. [Accessed 20 April 2025]. DOI 10.1259/bjr.20170577. Available from: https://dx.doi.org/10.1259/bjr.20170577
48. VALLADARES, Alejandra, AHANGARI, Sahar, BEYER, Thomas, BOELLAARD, Ronald, CHALAMPALAKIS, Zacharias, COMTAT, Claude, DALTOSO, Laura, HANSEN, Adam E., KOOLE, Michel, MACKEWN, Jane, MARSDEN, Paul, NUYTS, Johan, PADORMO, Francesco, PEETERS, Ronald, POTH, Sebastian, SOLARI, Esteban and RAUSCH, Ivo. Clinically valuable quality control for PET/MRI systems: Consensus recommendation from the HYBRID consortium. *Frontiers in Physics* [online]. 24 September 2019. Vol. 7, no. SEP, p. 474892. [Accessed 20 April 2025]. DOI 10.3389/fphy.2019.00136. Available from: www.frontiersin.org
49. KEENAN, Kathryn E., AINSLIE, Maureen, BARKER, Alex J., BOSS, Michael A., CECIL, Kim M., CHARLES, Cecil, CHENEVERT, Thomas L., CLARKE, Larry, EVELHOCH, Jeffrey L., FINN, Paul, GEMBRIS, Daniel, GUNTER, Jeffrey L., HILL, Derek L.G., JACK,

Clifford R., JACKSON, Edward F., LIU, Guoying, RUSSEK, Stephen E., SHARMA, Samir D., STECKNER, Michael, STUPIC, Karl F., TRZASKO, Joshua D., YUAN, Chun and ZHENG, Jie. *Quantitative magnetic resonance imaging phantoms: A review and the need for a system phantom* [online]. 1 January 2018. John Wiley & Sons, Ltd. [Accessed 20 April 2025]. Available from: https://onlinelibrary.wiley.com/doi/full/10.1002/mrm.26982

50. EFOMP. EFOMP's GUIDELINE - Quality controls in PET/CT and PET/MR. [online]. 2022. P. 1–62. [Accessed 21 April 2025]. Available from: www.efomp.org
51. PRICE, Ron, ALLISON, Jerry, CLARKE, Geoffrey, DENNIS, Michael, HENDRICK, R Edward, KEENER, Carl, MASTEN, Jeff, NESSAIVER, Moriel, OCH, Joe and REEVE, Donna. ACR - Magnetic Resonance Imaging Radiologist's Section MRI Technologist's Section Medical Physicist/MRI Scientist's Section QUALITY CONTROL MANUAL QUALITY CONTROL MANUAL Radiologist's Section MRI Technologist's Section Medical Physicist/MRI Scientist's Se. . 2015.
52. HENDRICK, R. Edward. Signal, Noise, Signal-to-Noise, and Contrast-to-Noise Ratios. In : *Breast MRI* [online]. Springer, New York, NY, 2008. p. 93–111. [Accessed 21 April 2025]. ISBN 978-0-387-73507-8. Available from: https://link.springer.com/chapter/10.1007/978-0-387-73507-8_7
53. YOUNG, I. R. MRI theory. In : *Encyclopedia of Spectroscopy and Spectrometry* [online]. Academic Press, 2017. p. 904–910. [Accessed 21 April 2025]. ISBN 9780128032244. Available from: https://www.sciencedirect.com/science/article/pii/B9780128032244002132?ref=pdf_download&fr=RR-2&rr=93c05dcfcb8fee43
54. IMAGING, Rapid. Gradient linearity. [online]. 2016. P. 2–3. [Accessed 21 April 2025]. Available from: https://mriquestions.com/gradient-linearity.html
55. ELSTER, Allen. Eddy currents. [online]. [Accessed 21 April 2025]. Available from: https://mriquestions.com/eddy-current-problems.html
56. STAFFORD, Roger Jason. *The Physics of Magnetic Resonance Imaging Safety* [online]. 1 November 2020. Elsevier. [Accessed 6 May 2025]. Available from: https://www.sciencedirect.com/science/article/abs/pii/S1064968920300519
57. AMERICAN COLLEGE OF RADIOLOGY. Acr position statement on quality control and improvement, safety, infection control, and patient education. *American College of Radiology* [online]. 2008. [Accessed 5 May 2025]. Available from: https://www.acr.org/Advocacy/Position-Statements/Quality-Control-and-Improvement
58. AAPM. *AAPM: The American Association of Physicists in Medicine* [online]. 2020. [Accessed 5 May 2025]. Available from: https://www.aapm.org/
59. AAPM Publications - AAPM Reports. [online]. [Accessed 5 May 2025]. Available from: https://www.aapm.org/pubs/reports/?s=Magnetic resonance imaging
60. ZIEGELBERGER, G., VECCHIA, P., HIETANEN, M., AHLBOM, A., ANDERSON, L. E., BREITBART, E., DE GRUIJL, F. R., LIN, J. C., MATTHES, R., PERALTA, A. P., SÖDERBERG, P., STUCK, B. E., SWERDLOW, A. J., TAKI, M., SAUNDERS, R. and VEYRET, B. *Guidelines on limits of exposure to static magnetic fields*. April 2009.
61. EDITORIAL TEAM. The invention of magnetic resonance imaging (MRI). *International Electrotechnical Comission* [online]. 2016. [Accessed 5 May 2025]. Available from: https://www.iec.ch/blog/invention-magnetic-resonance-imaging-mri
62. IEC 60601-2-33:2022 | IEC. [online]. [Accessed 23 May 2025]. Available from: https://webstore.iec.ch/en/publication/67211
63. STUPIC, Karl F., AINSLIE, Maureen, BOSS, Michael A., CHARLES, Cecil, DIENSTFREY, Andrew M., EVELHOCH, Jeffrey L., FINN, Paul, GIMBUTAS, Zydrunas, GUNTER, Jeffrey L., HILL, Derek L.G., JACK, Clifford R., JACKSON, Edward F., KARAULANOV, Todor, KEENAN, Kathryn E., LIU, Guoying, MARTIN, Michele N., PRASAD, Pottumarthi V., RENTZ, Nikki S., YUAN, Chun and RUSSEK, Stephen E. *A standard system phantom for*

magnetic resonance imaging [online]. 1 September 2021. John Wiley & Sons, Ltd. [Accessed 20 April 2025]. Available from: https://onlinelibrary.wiley.com/doi/full/10.1002/mrm.28779

64. ACR Medium MRI Accreditation Phantom - Sun Nuclear. [online]. [Accessed 20 April 2025]. Available from: https://www.sunnuclear.com/products/acr-mri-phantom
65. PEERLINGS, Jurgen, COMPTER, Inge, JANSSEN, Fiere, WIGGINS, Christopher J., POSTMA, Alida A., MOTTAGHY, Felix M., LAMBIN, Philippe and HOFFMANN, Aswin L. Characterizing geometrical accuracy in clinically optimised 7T and 3T magnetic resonance images for high-precision radiation treatment of brain tumours. *Physics and Imaging in Radiation Oncology*. 1 January 2019. Vol. 9, p. 35–42. DOI 10.1016/j.phro.2018.12.001.
66. Large/Medium Phantom Testing: MRI : Accreditation Support. [online]. [Accessed 6 May 2025]. Available from: https://accreditationsupport.acr.org/support/solutions/articles/11000061035-large-medium-phantom-testing-mri-revised-2-12-25-
67. DAVIDS, Mathias, ZÖLLNER, Frank G., RUTTORF, Michaela, NEES, Frauke, FLOR, Herta, SCHUMANN, Gunter and SCHAD, Lothar R. Fully-automated quality assurance in multi-center studies using MRI phantom measurements. *Magnetic Resonance Imaging* [online]. 1 July 2014. Vol. 32, no. 6, p. 771–780. [Accessed 5 May 2025]. DOI 10.1016/j.mri.2014.01.017. Available from: https://www.sciencedirect.com/science/article/pii/S0730725X14000216
68. ADJEIWAAH, Mary, GARPEBRING, Anders and NYHOLM, Tufve. Sensitivity analysis of different quality assurance methods for magnetic resonance imaging in radiotherapy. *Physics and Imaging in Radiation Oncology* [online]. 1 January 2020. Vol. 13, p. 21–27. [Accessed 7 May 2025]. DOI 10.1016/j.phro.2020.03.001. Available from: https://www.sciencedirect.com/science/article/pii/S2405631620300051
69. MCROBBIE, Donald W., MOORE, Elizabeth A., GRAVES, Martin J. and PRINCE, Martin R. Ghosts in the Machine: Quality Control. In : *MRI from Picture to Proton* [online]. Cambridge University Press, 2017. p. 166–182. [Accessed 7 May 2025]. Available from: https://www.cambridge.org/core/books/mri-from-picture-to-proton/ghosts-in-the-machine-quality-control/043E256A3317D0B72A214912AE6CD6D1
70. ZHUO, Jiachen and GULLAPALLI, Rao P. AAPM/RSNA physics tutorial for residents: MR artifacts, safety, and quality control. *Radiographics* [online]. January 2006. Vol. 26, no. 1, p. 275–297. [Accessed 20 April 2025]. DOI 10.1148/rg.261055134. Available from: https://www.researchgate.net/publication/7354707_MR_artifacts_safety_and_quality_control_AAPMRSNA_Physics_tutorial_for_residents
71. DONG, Qian, ADAMS, Zander, WATKINS, Ronald D., LEE, Brian J., CHANG, Chen Ming, SACCO, Ilaria and LEVIN, Craig S. Study of compatibility between a 3T MR system and detector modules for a second-generation RF-penetrable TOF-PET insert for simultaneous PET/MRI. *Medical Physics* [online]. 1 June 2023. Vol. 50, no. 6, p. 3389–3400. [Accessed 20 April 2025]. DOI 10.1002/mp.16354. Available from: https://www.researchgate.net/publication/369200756_Study_of_compatibility_between_a_3T_MR_system_and_detector_modules_for_a_second-generation_RF-penetrable_TOF-PET_insert_for_simultaneous_PETMRI
72. GARDNER, Edward A., ELLIS, James H., HYDE, Rosemary J., AISEN, Alex M., QUINT, Douglas J. and CARSON, Paul L. Detection of degradation of magnetic resonance (MR) images: Comparison of an automated MR image-quality analysis system with trained human observers. *Academic Radiology* [online]. 1995. Vol. 2, no. 4, p. 277–281. [Accessed 5 May 2025]. DOI 10.1016/S1076-6332(05)80184-9. Available from: https://pubmed.ncbi.nlm.nih.gov/9419562/
73. SUN, Jidi, BARNES, Michael, DOWLING, Jason, MENK, Fred, STANWELL, Peter and GREER, Peter B. An open source automatic quality assurance (OSAQA) tool for the ACR MRI phantom. *Australasian Physical and Engineering Sciences in Medicine* [online]. 29

March 2015. Vol. 38, no. 1, p. 39–46. [Accessed 5 May 2025]. DOI 10.1007/s13246-014-0311-8. Available from: https://pubmed.ncbi.nlm.nih.gov/25412885/

74. HENDRIKS, Janine, MUTSAERTS, Henk Jan, JOULES, Richard, PEÑA-NOGALES, Óscar, RODRIGUES, Paulo R., WOLZ, Robin, BURCHELL, George L., BARKHOF, Frederik and SCHRANTEE, Anouk. *A systematic review of (semi-)automatic quality control of T1-weighted MRI scans* [online]. 1 January 2024. Springer Science and Business Media Deutschland GmbH. [Accessed 24 May 2025]. Available from: https://pmc.ncbi.nlm.nih.gov/articles/PMC10761394/
75. JHAVERI, Kartik. *Image quality versus outcomes* [online]. 1 April 2015. John Wiley and Sons Inc. [Accessed 24 May 2025]. Available from: /doi/pdf/10.1002/jmri.24622
76. YANG, Xiangyu, LITTLE, Kevin, JIANG, Xia and HINTENLANG, David. Improvement in MR quality control workflow and outcomes with a web-based database. *Journal of Applied Clinical Medical Physics* [online]. 1 May 2020. Vol. 21, no. 5, p. 98–104. [Accessed 24 May 2025]. DOI 10.1002/acm2.12879. Available from: https://pmc.ncbi.nlm.nih.gov/articles/PMC7286007/
77. MAGNETOM Aera - Siemens Healthineers USA. [online]. [Accessed 21 April 2025]. Available from: https://www.siemens-healthineers.com/en-us/magnetic-resonance-imaging/3t-mri-scanner/magnetom-skyra
78. Siemens 3T MRI (Magnetom Skyra) – Echelon Health. [online]. [Accessed 21 April 2025]. Available from: https://www.echelon.health/facilities/aplio-500/
79. MAGNETOM Altea - Siemens Healthineers. [online]. [Accessed 21 April 2025]. Available from: https://www.siemens-healthineers.com/magnetic-resonance-imaging/0-35-to-1-5t-mri-scanner/magnetom-altea
80. MR Ingenia 3.0T | Philips Healthcare. [online]. [Accessed 21 April 2025]. Available from: https://www.philips.co.uk/healthcare/resources/landing/the-next-mr-wave/ingenia-prodiva#downloads
81. ETMAN, H. M., MOKHTAR, A., ABD-ELHAMID, M. I., AHMED, M. T. and EL-DIASTY, T. The effect of quality control on the function of magnetic resonance imaging (MRI), using American College of Radiology (ACR) phantom. *Egyptian Journal of Radiology and Nuclear Medicine* [online]. 1 March 2017. Vol. 48, no. 1, p. 153–160. [Accessed 9 May 2025]. DOI 10.1016/j.ejrnm.2016.12.003. Available from: https://www.sciencedirect.com/science/article/pii/S0378603X16302327
82. JEZZARD, Peter and BALABAN, Robert S. Correction for geometric distortion in echo planar images from B0 field variations. *Magnetic Resonance in Medicine* [online]. 1 July 1995. Vol. 34, no. 1, p. 65–73. [Accessed 15 May 2025]. DOI 10.1002/mrm.1910340111. Available from: /doi/pdf/10.1002/mrm.1910340111
83. Simulated images with geometric distortion representing EPI data with... | Download Scientific Diagram. [online]. [Accessed 15 May 2025]. Available from: https://www.researchgate.net/figure/Simulated-images-with-geometric-distortion-representing-EPI-data-with-motion-artifacts_fig2_221401617
84. ZHENG, Hong, QU, Xiaobo, BAI, Zhengjian, LIU, Yunsong, GUO, Di, DONG, Jiyang, PENG, Xi and CHEN, Zhong. Multi-contrast brain magnetic resonance image super-resolution using the local weight similarity. *BMC Medical Imaging* [online]. 17 January 2017. Vol. 17, no. 1, p. 1–13. [Accessed 15 May 2025]. DOI 10.1186/s12880-016-0176-2. Available from: https://bmcmedimaging.biomedcentral.com/articles/10.1186/s12880-016-0176-2